CHALMERS

Rapid heating and cooling of superconducting films with infrared lasers for ultra-low field magnetic resonance imaging

Master of Science Thesis in Biomedical Engineering

FARMAN ALI

Department of Signals and systems
Division of Biomedical Engineering

Department of Microtechnology and Nanoscience-MC2
Quantum Device Physics Laboratory

CHALMERS UNIVERSITY OF TECHNOLOGY
Göteborg, Sweden 2011
Master's Thesis

MASTER'S THESIS

Rapid heating and cooling of superconducting films with infrared lasers for ultra-low field magnetic resonance imaging

---

Master of Science Thesis in Biomedical Engineering

FARMAN ALI

Department of signals and systems
Division of

Department of Microtechnology and Nanoscience-MC2
Quantum Device Physics Laboratory

CHALMERS UNIVERSITY OF TECHNOLOGY
Göteborg, Sweden 2011

Rapid heating and cooling of superconducting films with infrared lasers for ultra-low field magnetic resonance imaging
Master of Science Thesis in Biomedical Engineering
FARMAN ALI

Master's Thesis
ISSN XXXX-XXXX
Department of Signals and Systems
Division of

Department of Microtechnology and Nanoscience-MC2
Quantum Device Physics Laboratory

Chalmers University of Technology
SE-412 96 Göteborg
Sweden
Telephone: +46 (0)31- 772 1000

Rapid heating and cooling of superconducting films with infrared lasers for ultra-low field magnetic resonance imaging

Farman Ali

Department of Signals and Systems

Department of Microtechnology and Nanoscience-MC2

Chalmers University of Technology Gothenburg

Sweden

Abstract

Ultra-low field magnetic resonance imaging (ULF MRI) is a promising technique in medical imaging. It is still in its initial stage of experiments around the world. Unlike normal MRI (1.3-3 tesla or higher), ULF MRI works in extremely low magnetic fields in the range of micro teslas. The weakness of this low field limits the output signal on magnetic field sensor and leads to a very low signal to noise ratio (SNR). In order to increase the SNR researchers use pre-polarizing pulses. The high transition temperature Superconducting quantum interference device (SQUID) is an ultrasensitive magnetic field sensor and is the heart of our ULF MRI system. Our SQUIDs are fabricated from high transition temperature superconducting films, in particular, Yttrium Barium Copper Oxide (YBCO) that has a high tendency to trap flux when exposed to strong magnetic fields. This phenomenon is problematic in the case of ULF MRI use. When the pre-polarization pulses are applied to the sample under study, flux becomes trapped in the SQUID sensor that contributes to higher noise levels and dramatically reduces the overall system sensitivity.

Therefore, the purpose of this project is to minimize the negative effects of flux trapping on our SQUIDs. The end goal is the demonstrated capability to heat the SQUID above its critical temperature with an Infrared laser pulse and subsequently cool it back to the superconducting state within a few milli to microseconds.

Key words: *ULF MRI, SNR, SQUID, flux trapping, YBCO*

List of Figures

Table of Contents

Acknowledgments

First of all I would like to thank Almighty GOD for giving me the strength to complete my thesis. I am very grateful to my examiner Prof. Mikael Persson for granting me this exciting opportunity to work with such a great team on this state of art project. I wish to express my deep gratitude and sincere regards to my supervisor Justin Schneiderman for considering me to work under his supervision, encouraging me and for teaching me even the very basics of lab work in very friendly environment, I am proud to be your student. I am deeply grateful to my supervisor Fredrik Öisjöen for arranging the instrument for experiments and helping and guiding me the setup of instrument, constantly standing with me and observing my results throughout the experimental work, and helping me find the very important research articles.

I would like to thank Alexei Kalabukhov for allowing me in his lecture and lab session arranged for other students and for his expert guideline and discussions on the project. Many thanks, to Hadi Arjmandi Tash for all his assistance, sharing his knowledge on the topic and for being a very good friend to me.

Finally I would like to thank my parents for raising me and support me during my education and encouraging me through ups and downs in life. Without their help and efforts it was not possible for me to complete my master degree.

All of you have given me the courage and the will power to achieve my goals and I am very thankful.

Chapter 1

Introduction

Detail knowledge of human brain requires high tech noninvasive imaging methods with best spatial and temporal resolution. There is no single system which could provide satisfactory results for the both. MEG and EEG both measure the neural activity of brain without any structure information, they measure neural signals with millisecond temporal resolution but spatial accuracy is not good because of the electromagnetic inverse problem. fMRI is functional imaging of brain has high spatial resolution but temporal resolution is very low because of slow hemodynamic response [1]. The combination of functional MEG and structural MRI is not that easy, MEG works with SQUID an extremely low magnetic field sensor, while MRI works in 1 - 3 T magnetic field, the image registration is more susceptible to errors, and their combination is beyond the current technological setup [1].

Superconducting quantum interference device (SQUID) is one of the most effective ultra-low magnetic field sensor, it can detect magnet field down to 10^{-15} T [2]. This amazing property makes it ideal for various applications. One of the examples of SQUID application is ultra-low field magnetic resonance imaging (ULF MRI) and magnetic encephalography (MEG). The ongoing project in the department of Microtechnology and Nanoscience-MC2 is to develop a combined ULF MRI that operates at ~100 μT and MEG that works in the range of femtotesla (fT); the advantage of this combined instrument is that both the signals for ULF MRI and MEG can be detected by the same SQUID sensor. It will avoid different errors caused by co-registration of functional and structural information of the brain by recording both with one and the same instrument [3] [1].

The ULF MRI technique employs pre-polarization pulses in order to increase the SNR of the images. With the application of pre-polarizing pulse, SQUID is more susceptible to flux trapping which is a big problem and one of hurdles for the advance development ULF MRI. This flux trapping phenomenon creates a circulating supercurrent and the output signal become noisy. There are some methods to get rid of this noisy effect, e.g. passing high critical current (I_C), making flux dams [4] and many more but most of them are not suitable with the ULF MRI technique and other are not fully tested yet. In high temperature superconductors (HTS) the flux remains trapped while the sensor is in the superconducting state. When its temperature goes above the critical point (characteristic temperature ~90 K) and it becomes normal (non-superconductor), the flux dissipates in the form of heat. Once it becomes normal it needs to be cool down rapidly to its base temperature (~77 K), to be ready for its routine operation.

The heating and cooling cycle will run with every pre-polarization pulse. The time of heating and cooling should be in the range of milli to micro seconds, because of the NMR pulse sequence perquisite and the NMR signal's exponential decay. The SQUID should become normal and cool back to the superconducting state to capture the NMR signal before it completely decays. This is the ultimate goal of this thesis. The SQUID heating and cooling cycle needs to be adjusted in parallel with the sequence of pre-polarization pulses as it is the main cause of flux trapping to avoid the loss of time and get the optimize sensitivity of the sensor.

1.1 Project description

An important aspect of the ULF-MRI system is the pre-polarization pulse, which has a tendency to trap flux in our sensors and thereby reduce their sensitivity. This issue can be overcome by rapidly heating the film during application of the pre-polarization pulse. This project would investigate the possibility to rapidly heat and subsequently cool our Yttrium Barium Copper Oxide (YBCO) SQUID sensors with an Infrared (IR) laser. YBCO is high temperature superconductor works at ~77 K which is the boiling point of liquid hydrogen. This property makes the way for the live tissues or biological samples to bring it near it without any problems and measure the desired data [5]. In this project, for robust heating and cooling the Infrared pulsed laser will be used in order to avoid extra heating of HTS film.

1.2 Outline

This study will describe the basic principles of SQUID operation, how to apply the best possible method to remove trapped flux from the SQUID sensor, and how to make sure the possibility to implement its application in ULF MRI without the bothering effect of flux noise.

In chapter 2 the basic theory of superconductivity, basic principle of SQUID, and its parameters will be discussed. Chapter 3 will describe the theoretical background of this project as whole that includes some relevant basics of ULF MRI, the noise problem in SQUID and how to cope with the situation in this particular case of ULF MRI. The subsequent chapter will explain the experimental setup, procedure and the results obtained will be summarized. Final chapter contain overall discussion and conclusion on the project.

Chapter 2

Theory

This project is based on SQUID sensor which is composed of superconducting material, so before going to describe the principle of superconductivity and SQUID, it will be good to go through a brief history of superconductivity. The discovery of superconductivity by H Kamerlingh Onnes in 1911 was the beginning of whole new chapter in the history of low temperature physics. Since then physicists and scientists have taken keen interest and lead this interesting topic to a new level. The striking features of superconductivity are the disappearance of electrical resistivity and the change of its behavior to external magnetic field (perfect diamagnetic behavior) below certain characteristic temperature. These changes due to superconductivity makes the superconductor materials ideal for various applications, but its wide application was restricted by the low T_C of the superconductors which is typically near the boiling point of liquid helium 4.2 K [6]. In late 1957 Bardeen, Cooper and Schrieffer proposed that superconductivity is the microscopic effect of electron condensation, which overcome the repulsion and bound into pairs like boson state. This is called BCS theory of superconductivity [7].

After Josephson postulation about Josephson junction in 1962 and the creation of Josephson junction in 1963 paved the path for the invention fast magnetic sensor. The invention of SQUID in 1964, and then the discovery high temperature superconducting materials having transition temperature above the boiling point of liquid nitrogen in 1986 compelled the scientist to think about its broad application. Yttrium Barium Copper Oxide ($YBa_2Cu_3O_{7-\delta}$) also YBCO is the most commonly high Tc material used in electronics due it suitable properties. Ultra-low field MRI is another emerging application of SQUID. However ULF MRI technique and application of HTS SQUID made up of YBCO thin film, is more susceptible to flux trapping noise in the SQUID sensor, to which this project will cope with.

In this particular chapter the basics of superconductivity, Josephson junction, SQUID and different parameters of SQUID will be discussed in detail.

2.1 Superconductivity

Tremendous feature of certain materials is that when their temperature goes down below a specific temperature called critical temperature (Tc) their resistance vanishes, this is called superconductivity. This phenomenon was discovered by Heike Kamerlingh Onnes in 1911. He was doing some experiments at low temperature when noticed that mercury become superconductor at 4.2 K and its resistance is vanished. He later received Nobel Prize in 1913 for

his excellent work in low temperature physics. The characteristic temperatures for low Tc materials are few Kelvin [8]. The measurement data got by Onnes is shown in the figure: 2.1 (a).

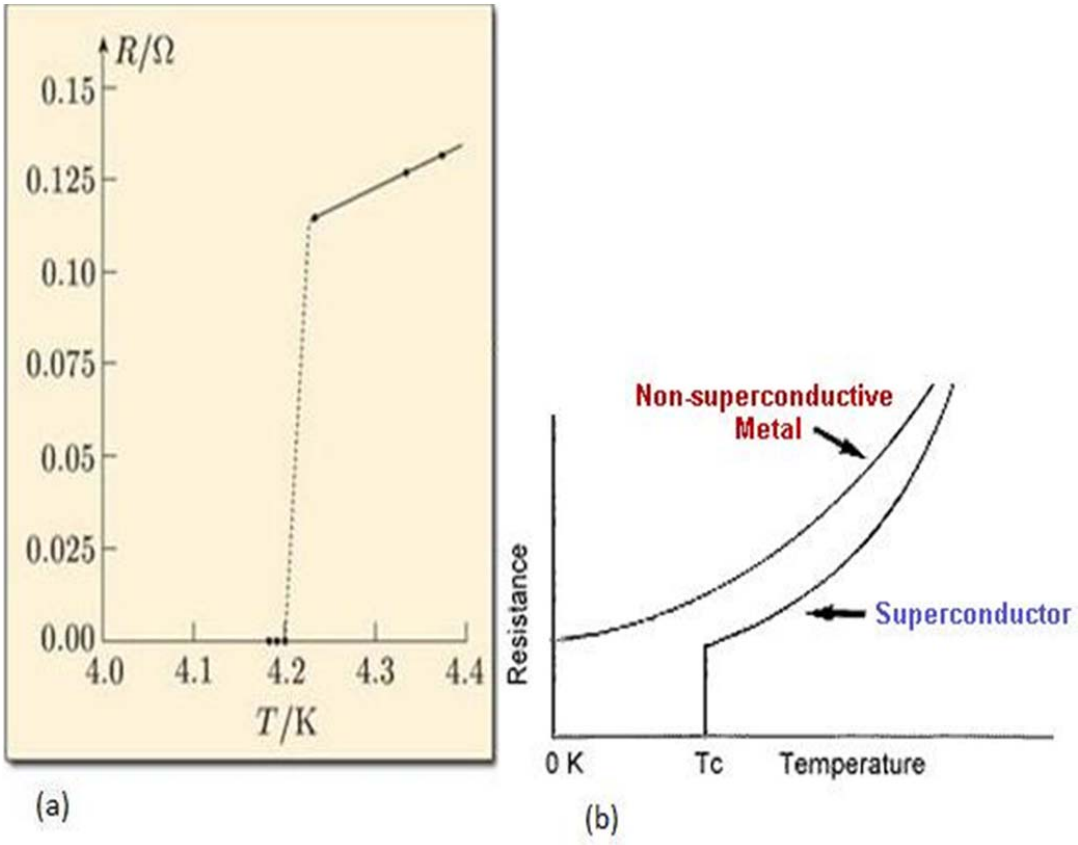

Figure: 2. 1 (a) Zero electrical resistivity of mercury measured by Kammerlingh Onnes in 1911. (b) Comparing the resistivity of superconductor and non-superconductor [6].

In 1933 Walter Meissner and Robert Ochsenfeld found that when a superconducting material changes from normal to superconducting state it completely expel the external magnetic field line from outside and behaves like a perfect diamagnetic material. The superconductor will not allow the magnetic field line to penetrate in it and will repel it. This is another striking phenomenon of superconductivity called Meissner effect. But this effect only will occur when the external magnetic field is below a certain threshold, if it gets stronger than a threshold level the magnetic field lines will penetrate through the material and the superconductivity will eventually lost. This kind of response of the superconductor has divided the materials in two types. Type 1 superconductor and type II will be discuss in more detail in this chapter later.

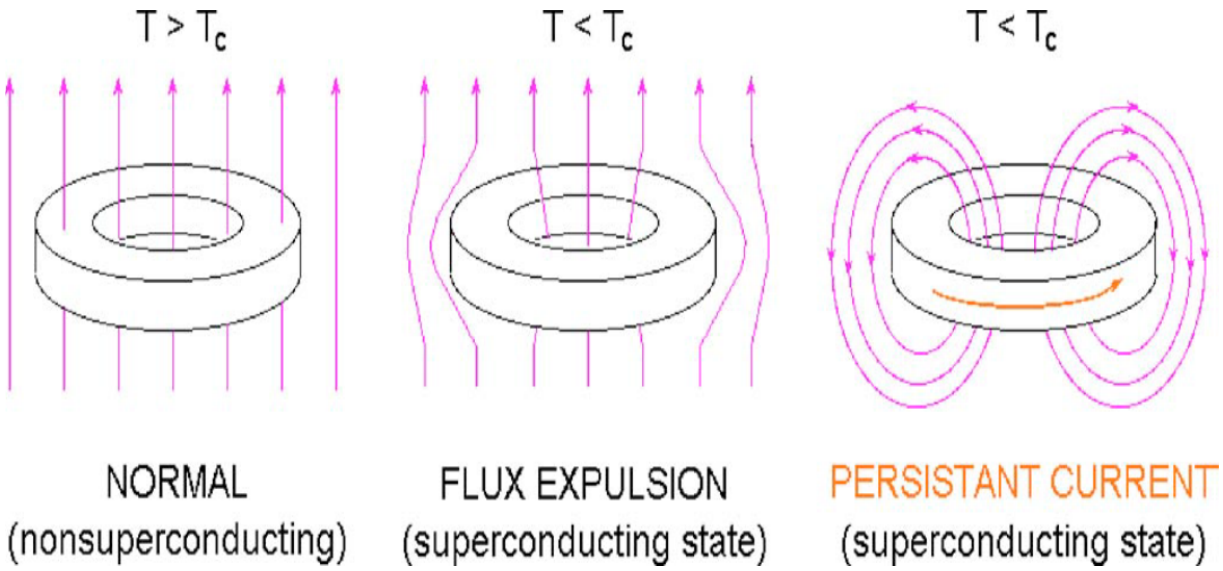

Figure: 2. 2 Meissner effect, where T > Tc the magnetic field lines passes through superconductor (normal state), T < Tc field lines are expelled from the superconductor [3].

In 1957 John Bardeen, Leon Cooper, and John Schrieffer proposed a new theory about superconductivity called microscopic BCS theory. Later they received Nobel Prize for their work in 1972. According to this theory when the electron moves in some kind of crystal they leave a cloud, a deformation cloud behind, this cause change in the electron core, this phenomenon introduces new positive charge which obviously attract nearby electrons to form a pair called cooper pair. This cooper pair travel without scattering and resistance free in nature thus creates superconductivity. However, this theory does not explain the superconductivity of high temperature superconductor [7].

Later in 1962 Brian D. Josephson a graduate student at Cambridge University discovered that if the superconductors were separated by an insulator or other non-superconductor there will be flow of charge through this insulator from one to another superconductor. This was another break through called Josephson Effect and won him Nobel Prize in 1973. This Josephson Effect has been used in electronic applications such as SQUID an extremely low magnetic field detector. There were different materials found to be superconductor below their critical temperature, most of them were below the boiling point of helium (4.2 K), which limited the wide application of superconductors, and therefore the curiosity was there to find some high temperature superconductors. In 1986 Georg Bednorz and Alex Müller were experimenting with ceramic materials they found Lanthanum Barium Copper Oxide (LBCO).This brittle ceramic material was synthesized and its critical temperature was 36 K. This invention was interesting because BCS theory had predicted the limitation for materials with critical temperature around 30K - 40 K because of thermal vibration [9]. This invention opened a new chapter of remarkable

high temperature superconductors' era and also won Georg Bednorz and Alex Müller a noble prize in the later year.

By this the scientist started to combine more ceramics to find more high temperature superconductor, in 1987 researchers from University of Alabama found Yttrium barium copper Oxide compound $YBa_2Cu_3O_{7-x}$ (YBCO), its critical temperature was 92 K which is above the boiling point of liquid nitrogen [10]. After this, new investigation and invention were made and even higher critical temperature materials were synthesized. At the present day the highest temperature superconductor is 138 K has been discovered.

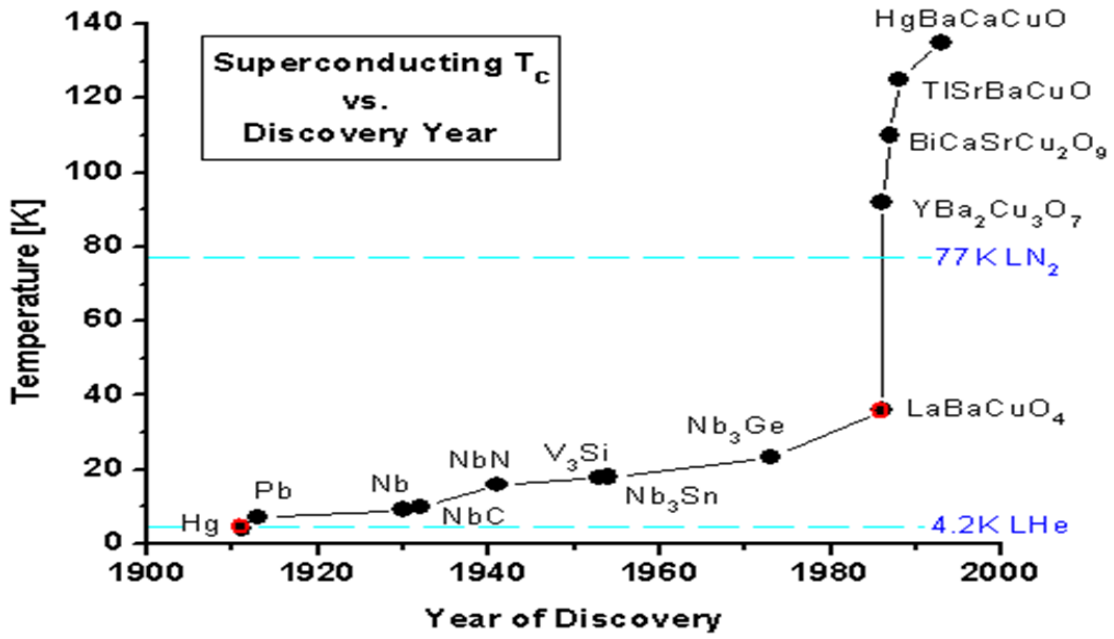

Figure: 2. 3 Evaluation of superconducting transition temperature from years 1900 to 2000, the red dots indicates the Nobel Prize winner for their work (Kammerlingh Onnes in 1913, Bednorz & Müller in 1987) [11].

2.2 Types of Superconductors

By applying high magnetic field when the material is in superconducting state it turn to normal state (non-superconductor). The characteristic value of magnetic field which turns superconducting state to the normal is called critical magnetic field Hc, and the threshold is H_{CT}. Based on this response to external magnetic field by superconductors they have been divided in to two classes, Type I, and type II. Type I superconductors stay in superconducting state in the presence of external magnetic field, when the threshold H_c value exceeds its limit the superconductor becomes normal. Critical magnetic field is function of temperature and it approaches to zero when the temperature is near to critical temperature (T_c) this relationship is shown below [12].

$$H_c = \begin{cases} H_{c0}\left[1-\left(\frac{T}{Tc}\right)^2\right] & T < T_c \\ 0 & T \geq T_c \end{cases} \qquad (2.1)$$

Here H_{c0} is the value of critical field at zero temperature.

Except vanadium, technetium and niobium, Type II superconductors are generally made up of more than one element while type I is generally composed of a single element [13]. Type II superconductor have two different level regarding magnetic field, the lower critical field Hc1, and Hc2 the upper critical field. In Hc1 state, a lower critical field when the external applied magnetic field is less than threshold value of magnetic field (H < Hc1) of the superconductivity, it stays in superconducting state, and behaves like type I superconductors [9]. When the external magnetic field goes above the H>Hc1 under the impression of Lorenz force law (FL) = (Φ_0 (jtr x H)/cH (here Φ_0 is magnetic flux quantum, J_{tr} is transport current, H is the applied magnetic field). A small number of electrons start to move in circle and create vortices having quantized trapped flux in the superconductor. The speeds of electron near the vortices have comparably high velocity and perpendicular to the magnetic field lines. As the motion of electron increased beyond certain critical value it destroys the state of superconductivity. Here superconductor goes above Hc1 and below Hc2 (Hc1 < H < Hc2). It is in mixed state, external magnetic field penetrate as vortices and this part act as normal while the other part is still behaving as superconductor. The value of each vortex has flux quantum of Φ_0 = 2.07x10^{-15} Tm^2. Above magnetic threshold value (Hc2) the superconductors completely becomes normal [14].

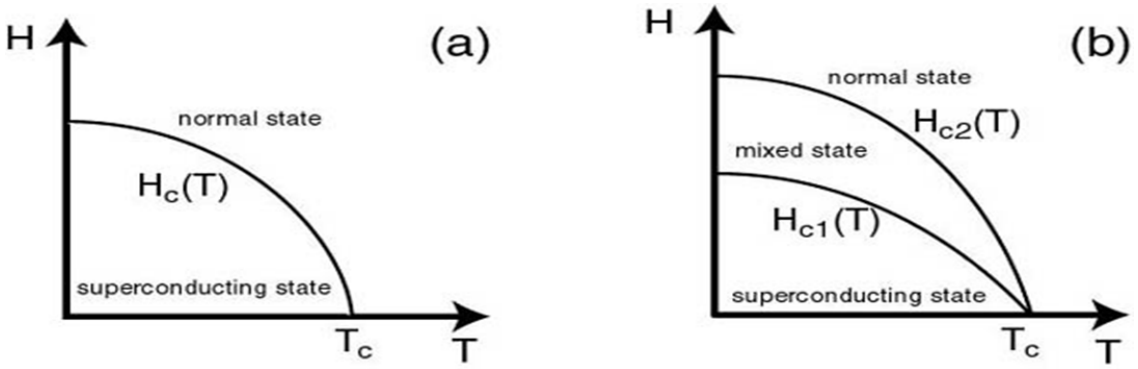

Figure: 2. 4 Critical magnetic field as function of temperature for (a) Type I superconductor, (b) Type II superconductors. The mixed state leads to the trapped vortices and thus noise in high Tc superconductors, the problem in our SQUID.

2.3 Properties of High Tc superconductors (YBCO)

In this project we will work on high temperature superconductor more specifically on yttrium barium copper oxide (YBCO), so it's important to understand the physical and chemical properties of it. YBCO ($Y_1Ba_2Cu_{3s}O_7$-x) has complex layered structure and highly anisotropic [14], having high current density and easy to make in single phase. It is the first superconductor with critical temperature (Tc) greater than 77 K which is the boiling point of liquid nitrogen. It is stable material with four element compound. Some typical specifications of YBCO are, Critical temperature 90 K and critical magnetic field 300 T, critical current density $J_c > 1$ MA/cm², and the dimensions of a single unit cell of YBCO are a = 3.82 Å, b = 3.89 Å, and c = 11.68 Å [15].

The mechanism of superconductivity is not very clear in it. The critical temperature of YBCO ($Y_1Ba_2Cu_3O_{7-x}$) depends on the value of x, its oxygen part. If the basic doping atom of oxygen comes down to 6.7 the Tc value will be between 55 - 60 K and even more below this oxygen content it will not remain as superconductor [16] or in other words $0 \leq x \leq 0.65$ it will be superconductor below 50 - 60 K and if x~.07 its critical temperature will go to 95 K [17]. YBCO's Cu-O covalently bonded with four oxygen atoms is considered to be responsible for its superconductivity [2]. Critical current density (Jc) is also important parameter of YBCO and it is used as function of temperature, Jc > 1 MA/cm^2 and it could be up to 10 MA/cm^2 [15].

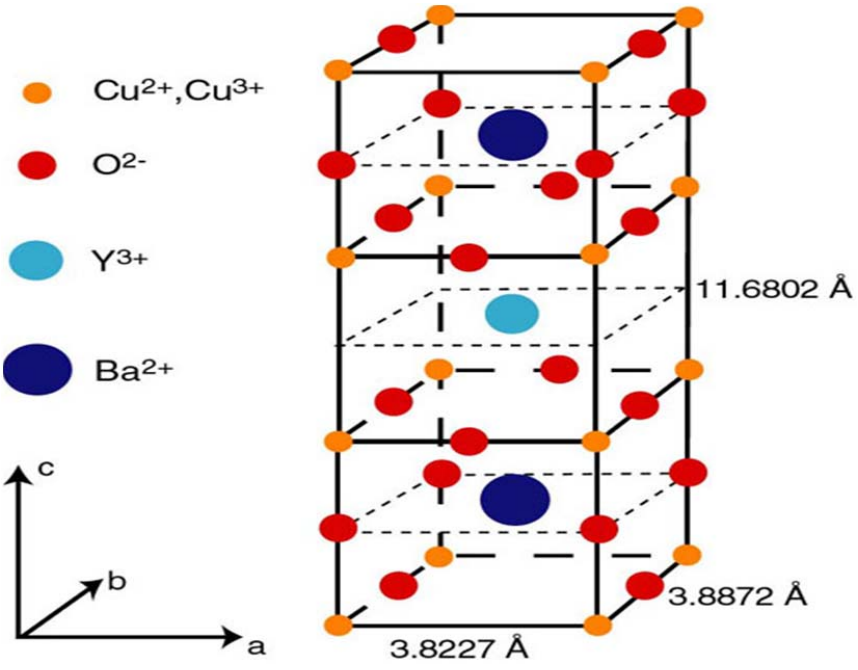

Figure: 2. 5 Elementary unit cell of HTS YBCO [15].

2.4 Josephson Effect

In 1962 Brian Josephson was working as graduate student in the Royal Society Mond Laboratory, Cambridge. He predicted that if two superconductors are connected through a thin insulating layer called weak link (superconductor-insulator-superconductor or S-I-S), this link will hold a supercurrent without application of any external voltage this effect is called Josephson Effect and the device is called Josephson junction. The critical current of the weak link will be less than that of superconductor part in order to create Josephson Effect. Following are the basic equations of Josephson Effect [18].

$$U(t) = \frac{\hbar}{2e}\frac{\partial \phi}{\partial t} \qquad (2.2)$$

In this Superconducting phase evolution equation, U (t) is the voltage across the junction$\Phi_0 \equiv \frac{h}{2e} = 2.7 \times 10^{-15} vs$ is the magnetic flux quantum, ϕ is the phase difference across the junction. Here if we represent the tunneling cooper pair through the insulator as wave function. All the cooper pair is said as single wave function has the same phase (phase coherent). And thus the tunneling can occur without the break of cooper pairs [19]. In DC Josephson junction the current I (t) is proportional to the sine of phase difference of the junction.

$$I(t) = I_c \sin(\phi(t)) \qquad (2.3)$$

In this Josephson or weak-link current-phase relation I (t) is current ϕ (*t*) = (ϕ1- ϕ2) is the phase difference and I_C is the critical current (constant) across the junction [20]. Josephson junction has many important application, e.g. it is used in SQUID for measuring a small flux change or called it flux to voltage transducer, other applications are microwave detector in the tera hertz range and also been used in rapid single flux quantum circuits [14].

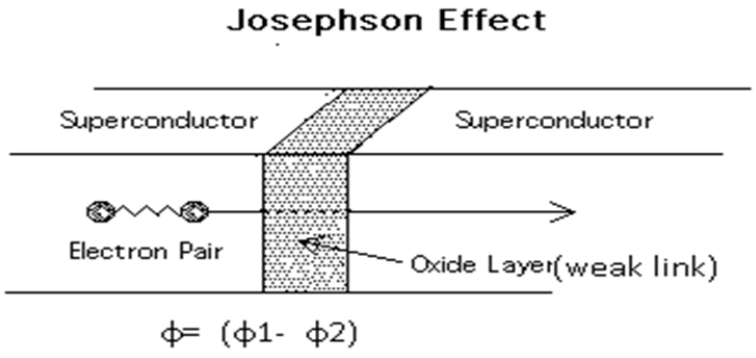

Figure: 2. 6 the passage of cooper pair in weak link from one superconductor to another.

2.5 Superconducting Quantum Interference Device (SQUID)

Before going to the experimental details of this study work it is important that the reader have a general understanding of the underlying processes and phenomenon responsible for the functioning of SQUID device. SQUID is ultra-sensitive magnetic field sensor; it is fast sensor and can responds to magnetic flux changes faster than nanoseconds [21]. ULF MRI is one of the applications of the sensor. Besides SQUID microscopy, biomagnetism, non-destructive evaluation, scientists are trying to explore and utilize the importance of SQUID in different applications [22]. There are two types of SQUID, Rf SQUID and DC SQUID, regarding to the application of DC SQUID in this project we will concentrate on it.

DC SQUID consist of two Josephson junctions connected in parallel to superconducting loop and each junction is connected resistively shunted to avoid the hysteresis on the I-V characteristics [figure 2.8 (a)]. It works on two phenomenon Josephson Effect and flux quantization [5] [23]. Flux quantization refers to the process when magnetic field applied to the SQUID below critical temperature (Tc) it expels the magnetic field line but some flux stay remain trapped within it and exhibit some weird properties. The value of this flux is not continuos. The flux enclosed by the superconducting ring is quantized in flux quantum $\Phi_0 = h/2e \approx 2.07\times10^{-15}$ Tm^2 where h is plank's constant and e is the electron charge [6] [22].

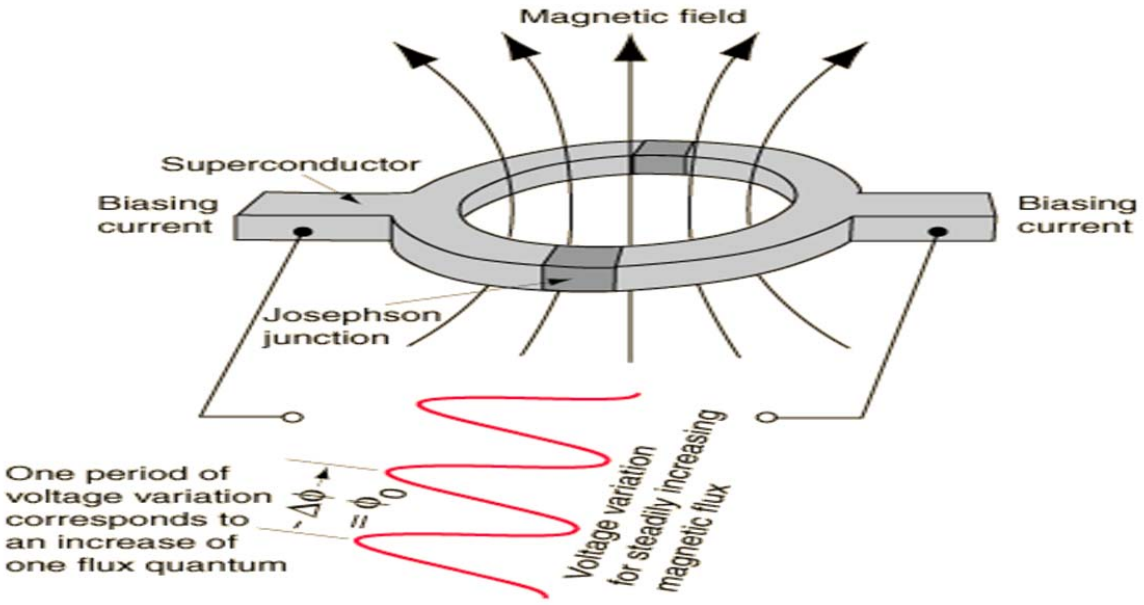

Figure: 2. 7 DC SQUID with two Josephson junction in the presence of external magnetic field and its periodic voltage [22].

When small external flux applied to the SQUID loop, it will produce current, results the magnetic field will cancel the flux. Now if the flux applied is slightly increased from $\Phi_0/2$ to Φ_0, mean half increment of its original value and the current will change its flow direction. Thus the critical current oscillates as function of flux change. In the presence of constant biased current I_b if magnetic flux changes it will cause a wave function change. This optimize current in one junction ($I_{total} = I_b + I_{screen} > I_C$) and on the other junction decreases the current ($I_{total} = I_b - I_{screen}. < I_C$ [6] . The voltage across the SQUID oscillates as a function of external flux (Φ) and this voltage in the form of periodic flux quantum Φ_0 used to give for feedback to the SQUID to cancel the flux [4]. Figure 2.8 b showing the I-V characteristics curve fluctuates between two state $\phi = n\,\phi_0$ and $\phi = (n+1/2)\,\phi o$. To measure the small change in the oscillation it is important to maintain a biased current with change in the amplitude and the external flux value, it should be like $(2m+1)\,\Phi_0/4$ where (m=1, 2, 3…). Thus the flux to voltage coefficient is maximum and the SQUID measure maximum change in voltage (δV) with small variation in flux $\delta\,\Phi$ [2] and it is called flux to voltage converter.

In short SQUID requires four things for operation; Bias current I_b, Modulation and signal, feedback and driver electronic for operation. The detected voltage if small, its amplification is done by semiconductors circuits. High Tc SQUID works on 77 K the boiling point of nitrogen typically uses as gradiometers to measure the gradient field. Its advantage as gradiometer is to reduce the effect of far distances noise as compare to magnetometer [24].

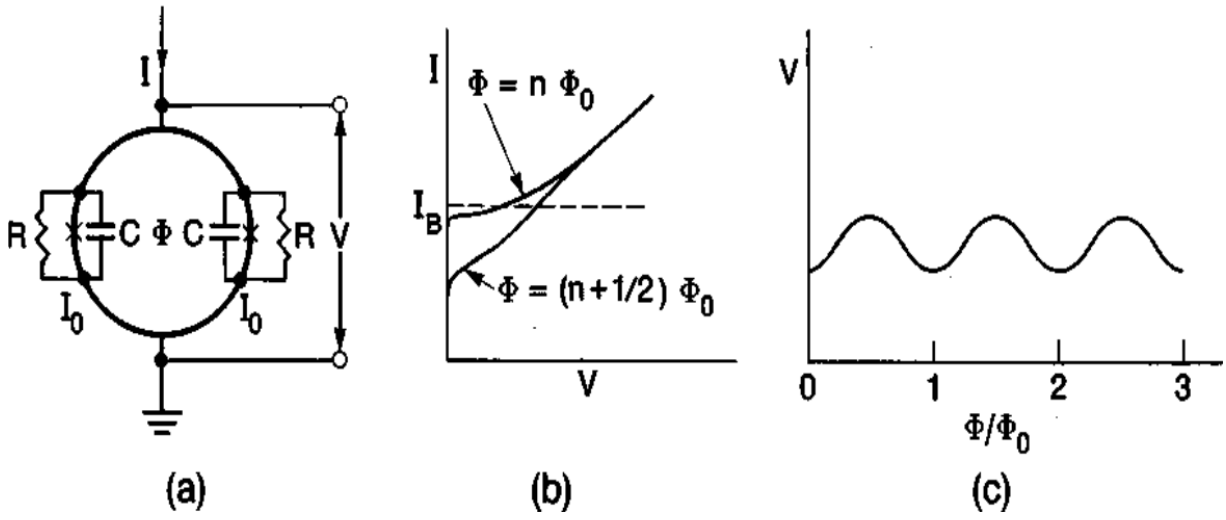

Figure: 2. 8 The DC SQUID: (a) Electrical schematic of SQUID (b) I-V characteristic curve with different applied flux with very weak hysteresis(c) Periodic voltage response or modulation due to flux (V vs $\boldsymbol{\Phi}/\boldsymbol{\Phi}_0$ at constant bias current Ib) [25].

2.6 Parameters of DC SQUID

Two parameters are very important to know the characteristics of SQUID. One is the modulation of critical current, the current modulation parameter β_L, where $\beta_L \approx 1$ for enhance SQUID resolution in operational form and the other is Stewart-McCumber parameter (or hysteresis parameter) β_C which is damping measurement of Josephson junction [25].

$$\beta_L = \frac{2LC_I}{\Phi_0} \qquad (2.4)$$

$$\beta_c \equiv \frac{2\pi R_n^2}{\Phi_0} \qquad (2.5)$$

Other important parameter is the effective area which increases its sensitivity. In order to make a DC SQUID more sensitive and measure very small change in magnetic field or flux, it is important to increase the loop area. With increase in the loop area A and small change in the magnetic field ΔB will cause prominent change in the flux $\Delta\Phi = A \cdot \Delta B$. SQUID inductance L is proportional to the ring surrounded area. The problem coming here L is needed to be small and the area should be large, so we are having conflicting statement. Actually this is done by using diamagnetic behavior of superconductor instead of using washer [26]. For high temperature SQUID the inductance is ranging from 50 pH < L < 100 pH [25]. Figure: 2.9 showing equivalent circuit of dc SQUID with large area and grain boundary Josephson junction. Here the inductance could be determined by the ring current. The best example is SQUID transformer with large effective area will be discussed in the next section [26].

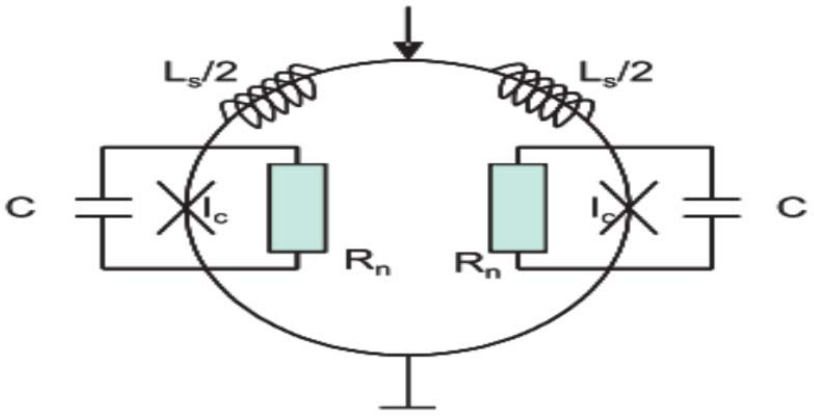

Figure: 2. 9 Showing equivalent circuit of DC SQUID [27].

The SQUID assembly shown in the figure below to improve the sensitivity of SQUID, it is coupled with a loop with large area. It is made up of Nb wire or Nb thin film integrated with the SQUID, which is connected to multi turn coil, is called flux transformer. By applying magnetic field, supercurrent circulates in the loop and the flux coupling occurs. Typical flux transformer has noise 1 $fTHz^{-1/2}$ [2]. The high input impedance as compare to SQUID impedance allows it to have larger area of the loop. The effective area A_{eff} of magnetometer is

$$A_{eff=}A_p M_i/(L_i + L_p) \pm A_{SQUID} \qquad (2.6)$$

Here A_{SQUID} is the area of the SQUID washer, A_P and L_P are the area and inductance of the pickup loop, respectively, and L_i is the input coil inductance. $M_{i\ =}\ \alpha\ (LL_i)^{1/2}$ Is the mutual inductance between L_i and SQUID inductance L [22] [28]. The other method to enhance the sensitivity of flux transformer is to connect the N number of loop in parallel with small inductance and effective area A_{eff} large. The advantage is, it can be placed in magnetic field in higher temperature comparably to SQUID (not limited to the exact temperature environment of SQUID) if the pickup loop is not superconducting material [22].

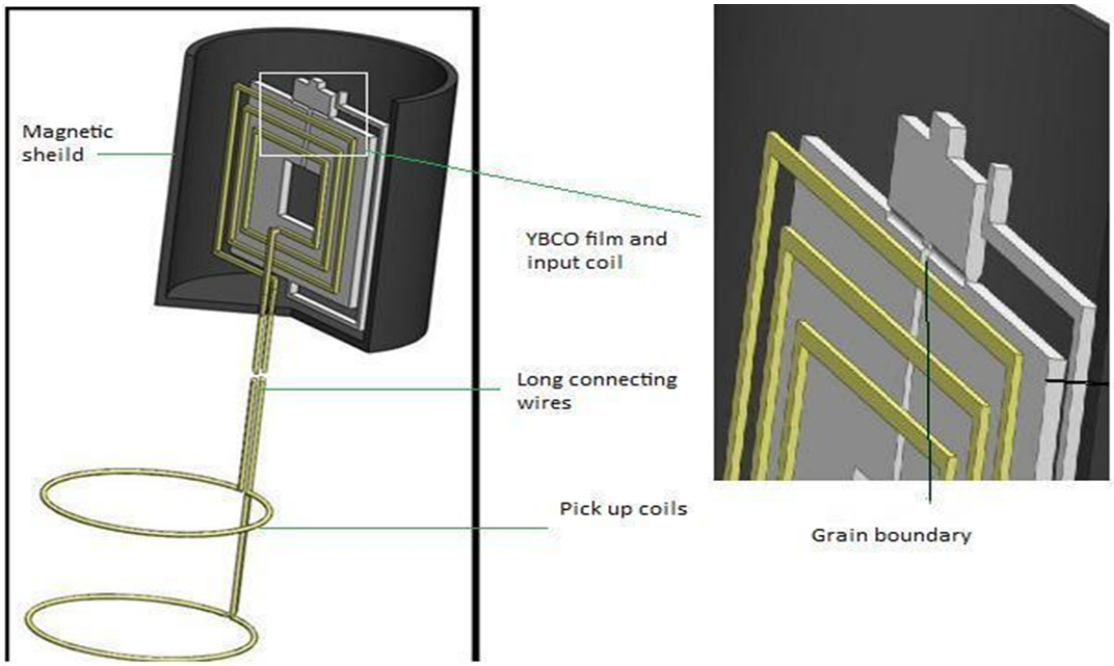

Figure: 2. 10 Showing SQUID assembly inside magnetic shield, Pick-up loops, connecting wires and input coil together compose flux transformer [4].

2.7 HTS Josephson Junctions and SQUID Fabrication

There are different types of high Tc Josephson junction like bicrystal junction grain boundary, biepitaxial, step edge, and ramp edge junction's fabrication of HTS. Some are very successful but the typical application requirement is also an important issue. For example the ramp edge has low I_cR_n product [29], step edge having unsettled transport and noise issues and excess current exhibition in the I-V characteristics [23]. There are a few other things like nonhysteretic I-V characteristics, high yield, how easy to get rid of noise issues, stability etc. to be consider before the fabrication. Some of these requirements are compatible with low Tc junctions by the Nb-Al_2O_3-Nb trilayer technology and there is no such technology present for high Tc available [23]. Here in this project work, grain boundary junction fabrication method has been used for the simplicity and reproducibility to realize the junction [30]. YBCO is highly anisotropic superconductor and due to this, the coupling of superconductor creates new type of weak link. This phenomenon is the reason of developing a very straight forward method of grain boundary junction. The SQUID in this project was fabricated in clean room facilities of the Chalmers department of Microtechnology and nanoscience MC2. The SQUID is made by depositing YBCO on strontium titanate oxide (STO) substrate with misorientation angles (24^o in this work or 30^o commonly) with typical critical current density (J_c) 10^4 - 10^5 A/cm^2 of bicrystal junction, which then leads to the patterning of narrow bridges with a very popular method of pulse laser deposition (PLD) has been applied for the fabrication of SQUID [31].The surface roughness YBCO can be find by atomic force microscopy. The advantage of this method (PLD) is to keep preserve the film composition safe, while cluster formation on the film surface is its drawback. The PLD system of growing YBCO thin film is based on Kr/F excimer laser with wavelength 288 nm and pulse duration 20ns [30].

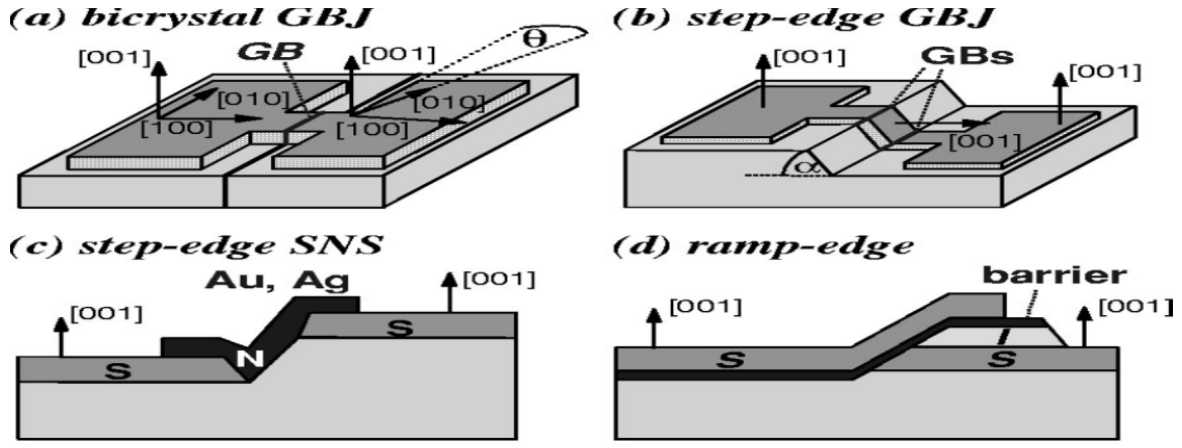

Figure: 2. 11 Different types of high-Tc Josephson junctions [23].

2.8 SQUID readout

DC SQUID is flux to voltage transducer, a very minute change in flux $\delta\Phi$ could produce considerable voltage change $\delta V = V_\Phi \delta\Phi$ here $V_\Phi = \delta V/\delta\Phi$. The SQUID operated in flux lock loop (FLL), the small change between the SQUID voltage and biasing voltage is passed through an amplifier, integrated and then return to a feedback coil. The signal is send to the feedback coil, which is magnetically coupled with SQUID through feedback resister R_f to cancel the flux in the SQUID. The function of R_f is to avoid the feedback impedance or to make it negligible in our desired range of frequency. The voltage V_f in the resister totally depends on the applied flux. The main problem coming in the SQUID readout is the linearization of transfer function without the addition of noise. In the case of DC SQUID used for low temperatures the current fluctuations, low frequency noise is removed by reverse biased current method [22] [32].

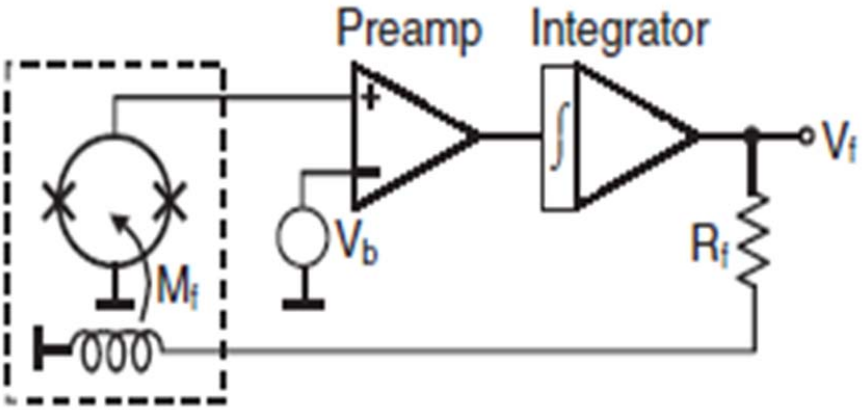

Figure: 2. 12 Basic flux lock loop circuit for the SQUID read out. The dashed lines show the SQUID area related to cryostats [32].

Chapter 3

Theoretical background of the project

Since this study work is a part of our MEGMRI project. It is important to have an idea about how ULF MRI works and how the flux trapping phenomenon occurs in the SQUID which is made up of YBCO film.

In the previous chapter we discussed the basic of SQUID, principle of operation etc. This chapter will describe in detail the basics of ULF MRI, and how the SQUID work with it, where and what kind of noise problems we were facing and how to cope with it?

3.1 Basics of ULF MRI

Magnetic resonance imaging (MRI) is very good noninvasive tool for detail study (Anatomy and physiology) of the human body. When a body is placed in magnetic field B_0 in z direction, All proton will align with or in opposite direction of magnetic field with energies – γh – $B_0/2$ and + γh – $B_0/2$. When radio frequency (RF) pulse applied on it, the alignment will disturb and it will start to precess about B_0, at Larmor frequency $\nu_0 = \gamma/2\pi\ B_0$ where γ is gyro magnetic ratio and γ/2π = 42.58 MHz/tesla. The magnetic moment is $M_0 = N\ \mu_p^2 B_0/k_B\ T$ with limitation $\mu_p\ B_0 << k_B\ T$, where μ_p is the magnetic moment of proton, K_B is Boltzmann's constant and T is the temperature (K). The oscillation of proton generates magnetic field and the coils around convert it to voltage and send it for image acquisition. For 3D image there different coils generate a unique magnetic field and after signal encoding one can create a complete image. In the presence of static magnetic field B_0 when we apply RF pulse π/2 in the Z direction, the M_0 precess about B_0 at frequency of ω0/2π, the M_0 precession followed by two relaxation times T1 the longitudinal relaxation (towards Z axis) and T2 the transverse relaxation time or spin-spin relaxation time (dephasing proton spin). T1 relaxation time is maximum in low field [33] and it is one of the advantages of ULF MRI because the contrast between two different tissues t_{1a} and t_{1b} depends on the difference between their relaxation rate: $1/t_{1a} - 1/t_{1b}$, in some kind of tissues this difference is maximum on low field (Microtesla) f_0<10 kHz [2]. After π/2 pulse, with specific time T a π (180^0) pulse applied in the y axis to cause 180^0 flip of M_0. The spin echo produces at time 2 t after [2] [33] [34].

Current trend of MRI works on magnetic field from 1.5 to 3 tesla [2][8]. Its spatial resolution is high but temporal resolution is low. More expensive and Patients with metallic implants cannot acquire the usefulness of the technology. On the other hand these high field (1.3 - 3 teslas) instruments cannot be combined with functional instrument (MEG and EEG) for brain imaging [1]. T1 weighted contrast is much better in low field and high magnetic relaxation dispersion of

tissues in low field is very good option for contrast improvement. So the curiosity automatically compels us to think about the development of low field MRI. Unlike high field MRI, it does not require extremely high field homogeneity, because low field is already homogenous on absolute scale [1]. Normal MRI has three kinds of gradient coils, an RF pulse transmitter and receiving coils and magnetic field coil. The same kind of setup is used for ULF MRI, only the static field B_0 reduces to micro tesla and the addition of pre-polarization pulse coils, and other different coils to cancel unnecessary magnetic field from outside. The receiving sensor is SQUID, a very low magnetic field sensor [2].

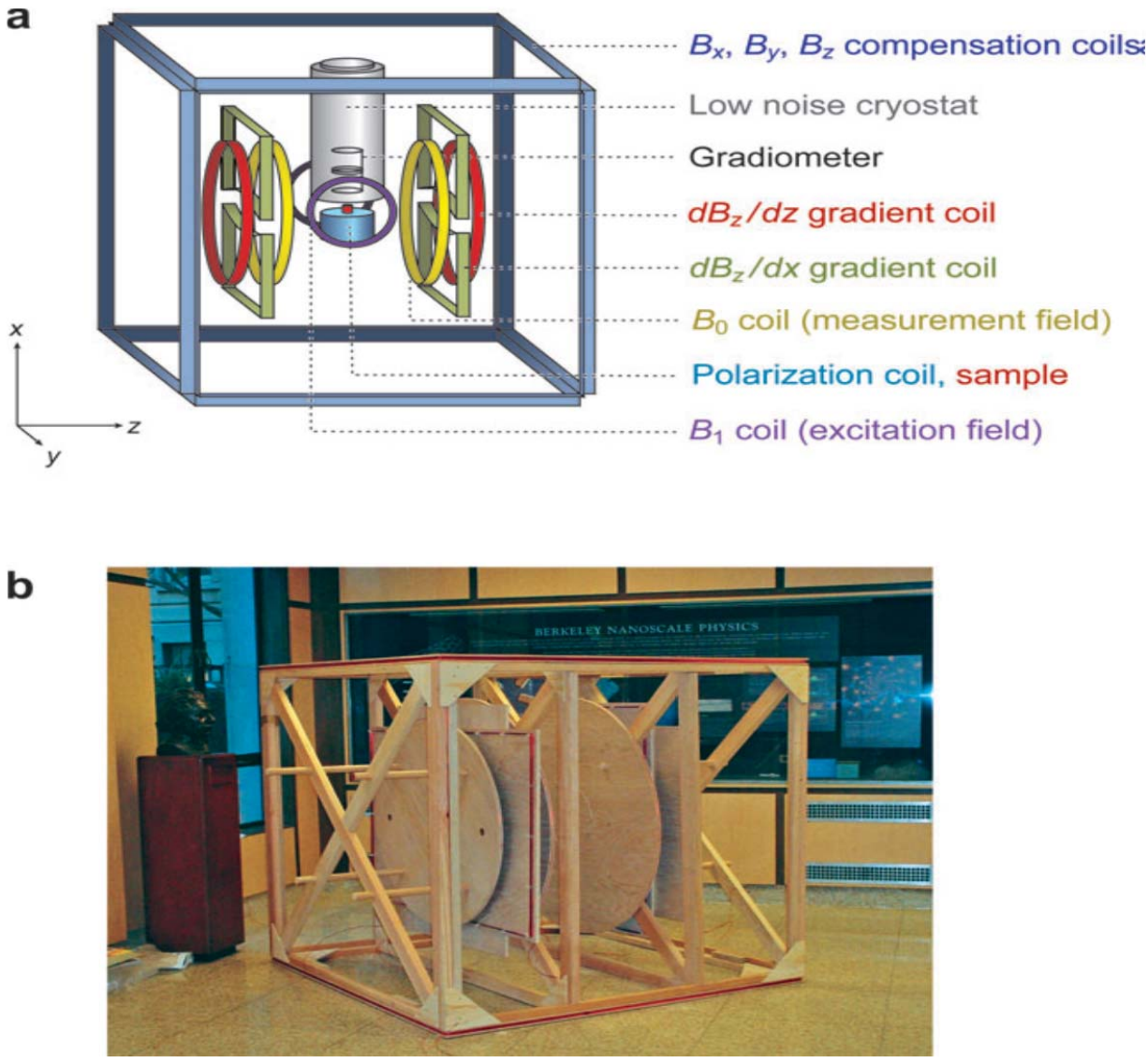

Figure: 3. 1 (a) Different coils, setup with cryostat and sample holder (b) Structure for coils assembly made up of wooden materials [2].

3.2 Pulse Sequence of Ulf MRI

ULF MRI is a new technique under research and different pulse sequence methods have been used for image acquisition. Here I will explain the Zotev and Clark approaches while drawing comparison between them to understand the pulse sequence of ULF MRI and because we will try all possibilities for our research in the area. The pulse sequence by Zotev et al starts with the pre-polarization pulse Bp applied for 1 s and then removes it before the measurement field B_m applied. The measurement field Bm is perpendicular to the direction of pre-polarization pulse. The image measurement process is undertaken inside the magnetic shielded room in order to avoid any extra magnetic field or background noise. For 3D image the phase encoding gradient Gx and spin precession with gradient Gy is performed, the echo signal is generated by the method of reversal static field without the use Rf pulses which is the simplest method for ULF MRI instrumentation used by Zotev et el [1]. Typical ULF MRI parameters used by Zotev et al in their experiment, Bp = 30 mT, B_m = ± 46 μT, Gx = ± 140 μT/m, |Gz| ≤ 140 Bp = 30 mT with 1 s time on, off pre-polarization pulse [33].

Pulse sequence for 3D image with specifications used by Clark et al are different, they used Rf 90^0 and 180^0 pulses to get the lattice relaxation t1 and t2 times. A typical pulse sequence consist of static or measurement field B_m = 132 μT and will remain turn on continuously. The pre-polarization pulse Bp ~85 mT field turns on for the period of 15 ms in x axis. A π/2 (5.5 kHz) pulse with time delay t_d and then π pulse, with time delay T will apply. The time between π/2 and π pulse is t. In the figure 3.2 in the signal free induction decay is result of π/2 pulse and the echo causes by the π pulse. The gradient pulses Gx ≡ ∂Gz/∂x (frequency), Gy ≡ ∂Bz/∂y and Gz ≡ ∂Bz/∂z (phase) are used for 3D encoding. The frequency gradient encodes after each 90^0 and 180^0 pulses during the whole measurement, while the phase encoding pulses applied briefly between π/2 and π measurement process [2]. The frequency space and phase encoding are given below

$$\omega(\mathrm{x}) = \gamma(\beta_0 + xG_x) \qquad (3.1)$$

$$\Delta\phi(z) = \gamma z G y \tau, \qquad \phi(y) = \gamma y G z \tau. \qquad (3.2)$$

Where ΔΦ is the phase, τ is the time of the given encoding pulse.

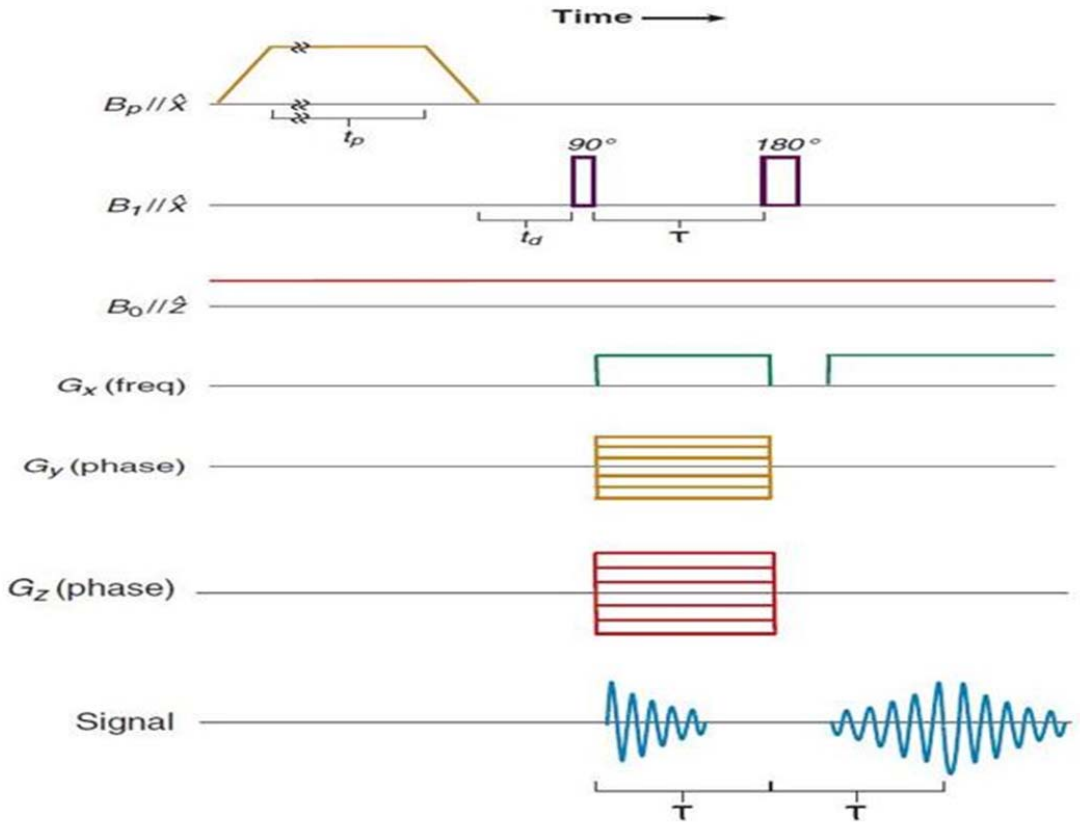

Figure: 3. 2: Pulse sequence by Clark et al for ULF MRI, with parameters 132 µT (proton Larmor frequency 5.6 kHz), using a polarizing field of 85 mT, the frequency encoding gradient was 240 µT m^{-1} [2].

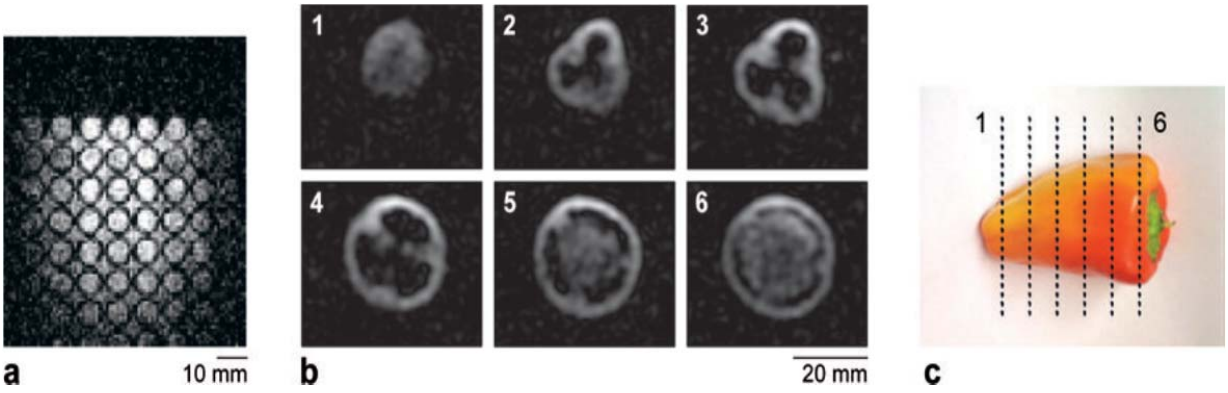

Figure: 3. 3. (a) Two-dimensional image of water in a multiwall with B0 = 132 µT, field gradient = 240 µT/m, and Bp = 85 mT, (b, c) Three-dimensional image of a whole bell pepper, acquired with B_0 = 132 µT, field gradient = 120 µT/m, and *Bp* = 60 mT [2].

3.3 Flux trapping in YBCO and ULF MRI

Our SQUID is made up of YBCO, a thin film and very good high critical temperature type II superconductor having transition temperature above boiling point of liquid nitrogen. It is important to know the nature of YBCO thin film and the flux trapping phenomenon that affect the performance of our SQUID in ULF MRI. When the external magnetic flux passes through a superconducting material, some flux will trap inside the superconductor during its superconducting state [4] [22]. As long as the temperature of the superconductor stays below its critical point the flux will remain inside. It is well a known fact that in response of magnetic field, the increasing critical flux value enters in to the superconducting film in the form of Josephson vortices, and trapped at the grain boundaries. There are also some chemical inhomogeneities appear which change the free energy in the superconductor and causes pinning of the vortices, leads to high mobility of flux lines causes low critical current J_C density [35]. So this flux pining comes from the superconducting grain of the film, impurities and geometry (topological defects) [36] of the materials, high critical temperature, large anisotropy and short coherence length. This entrapped flux creates a circulating supercurrent [37], due to this supercurrent the total flux passing through the HTS superconductor does not show its characteristic change. This is an unwanted effect in some high sensitive measurements system like ULF MRI [4].

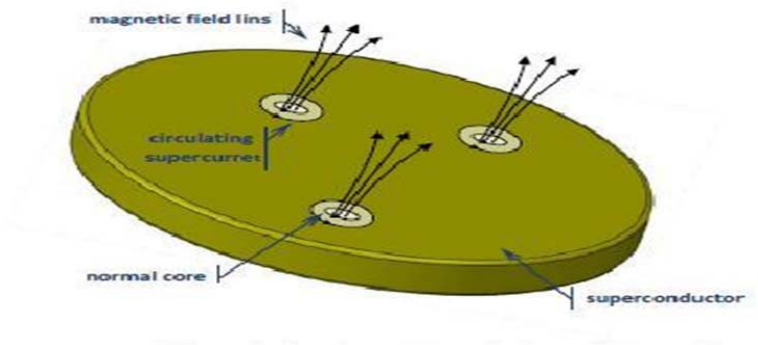

Figure: 3. 4 Magnetic field lines passing through and flux trap inside the superconductor [4].

Flux trapping is very important phenomenon in superconductivity specially with the combination of Meissner Effect and flux trapping, leads to magnetic levitation which is then utilized in many important application. But in some cases like ULF MRI, where high accuracy and sensitivity requires, flux trapping is a noisy effect. By consideration of flux trapping that causes less sensitivity, various methods have been applied to suppress or minimize the flux trapping effects. For example the impurities in superconductor, crystal structure defects that attract more vortices pinning, can be removed to avoid flux trapping. Similarly pickup coil is a highly

magnetic field sensor where the loop in connection with input coil of SQUID with small hole has low tendency of flux trapping [38]. To restrict the freely movement of vortex by making flux trapping sites called antidotes [39], weak link or flux dam, narrowing the width, slotting structure in grain boundary and many other under the research to minimize the flux trapping in the film [31]. Since MEG and ULF-MRI measurement requires pin point accuracy and robustness of SQUID as magnetic flux sensor or flux to voltage transducer without flux noise, so the above mentioned method help but don't seems to eliminate the problem altogether when the pre-polarization field strength is above 10 mT. To achieve the best SQUID performance and avoid the noise problem in the proposed method we have to heat up the SQUID sensor to its characteristics temperature and then rapidly cool it to the base temperature using infrared laser. By heating the film, the flux will dissipate to the surrounding in the form of heat and the SQUID will become normal. Before recordings are performed, the SQUID must be allowed to cool back below its critical temperature and become superconducting again. This whole process should be done in fraction of second i.e. milli seconds get ready the sensor and to conduct the next cycle process.

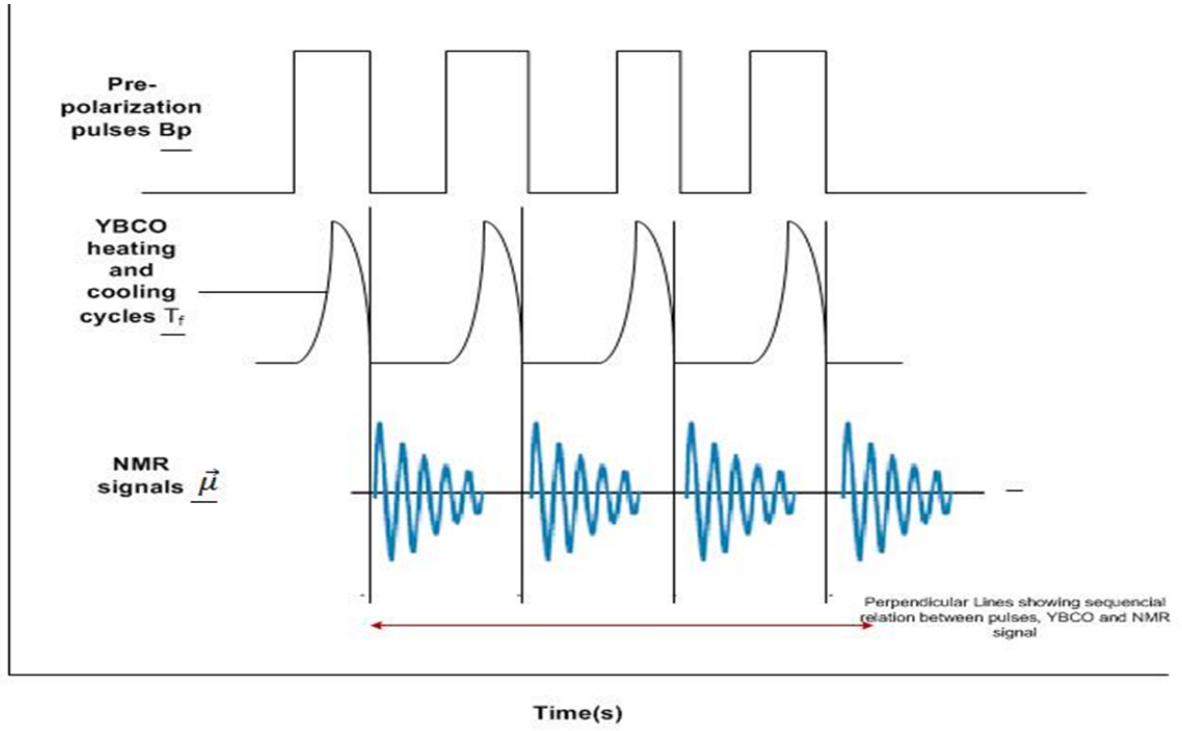

Figure: 3. 5 showing the theme of this thesis, the sequential relation between fast heating and cooling of superconductor film in coordination with the repetition of Pre-polarization pulses, to get it ready for flux de-trapping and catch up the NMR signal after cooling of superconductor film.

3.4 Peak Absorption wavelength Ranges of YBCO Film and Laser Selection for the project

Before starting our experimentation it was the question which wavelength laser would be the best for sharp heating of the film and how to manage the power of the laser according to the requirement. We know the optical absorption spectrum of YBCO ranges from 2000 cm^{-1} to 10000 cm^{-1}, HL Dewing and EKH Salje, experiments shows that the peak absorption of YBCO is 5500 cm^{-1} (1818 nm). Figure 3.6 b, showing the plotted integrated intensity of laser light as function of temperature where the peak absorption is 5500 cm^{-1} mostly at critical temperature [40]. For the power requirement we noticed the YBCO is ceramic material and have thermal damaging threshold greater than 10 W which is very high enough and there was no need to worry about our SQUID sensor damage because the maximum laser power used in this experimental work is 1000 mW.

We had to find the laser in the wavelength near 1800 nm, in this experimental work we used Infrared laser with 1250 nm wavelength range which good enough and near the ideal range.

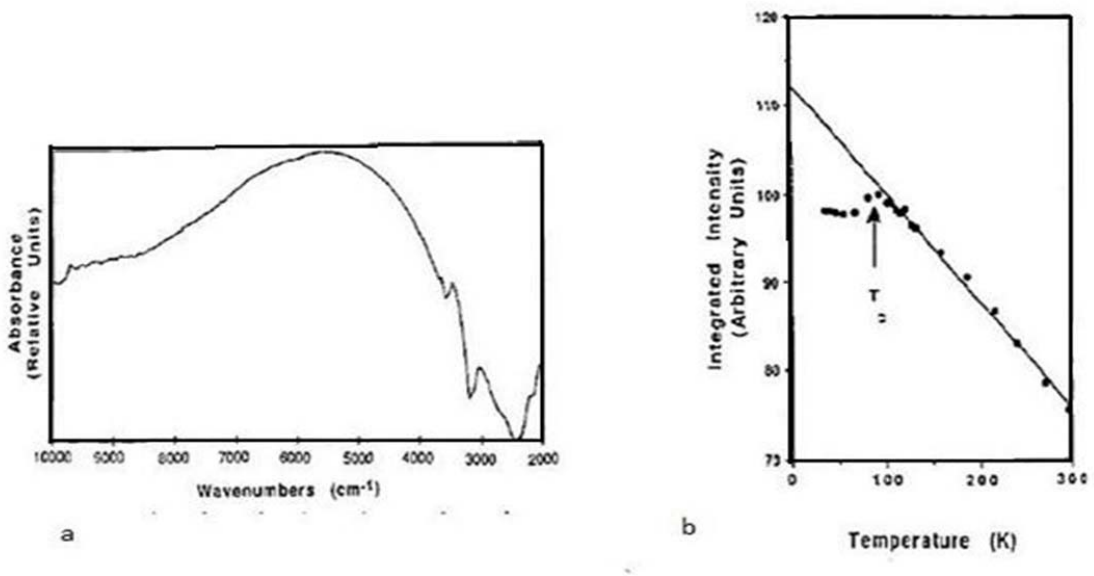

Figure: 3. 6 (a) The infrared absorption spectrum of YBCO between 2000 cm^{-1} - 10000 cm^{-1}, the peak absorption is 5500 cm^{-1}. (b) The integrated intensity of the infrared absorption peak is near 5500 cm^{-1} in YBCO and is plotted against the temperature, showing phase transition [40].

Chapter 4

Experimentation and results

The main components of experimentation setup were cryostat, Infrared laser and radio frequency shielded room with feedback electronic control system outside the room. We used three different lasers to test the response of SQUID and obtained the best results. Labview software was used for the monitoring of our real time results.

This chapter will present the detail of the experimentation setup, the types of instruments we used, and the results which obtained during this study.

4.1 The experimental setup

The first step toward the experimentation was to set up a cryostat and apply the low power 10 mW laser 850 nm wavelengths to avoid the hazardous effect of high power laser and just to see how much response is giving by the SQUID to laser heating. Though it was very low power and even there was no focusing lens but some response was noted and it was the first hope to go ahead for some higher power laser. Similarly we used another laser with maximum 200 mW multi-mode fiber optic, continuous waves and its heating was good as compare to previous one but the time it would take to start radiation and heating time was longer then expectation, the reason is multi-mode fiber with no focusing lens and totally manual control laser radiation (power on off by hand).

The actual setup of cryostat is given in the figures 4.1 and 4.2. It is fiber glass reinforced epoxy thermostat body to hold liquid nitrogen inside it. Between the liquid nitrogen holding chamber and outside fiberglass wall there is vacuum chamber strong enough to hold high vacuum for the best insulation i.e. to prevent heat exchange between outside environment and liquid nitrogen chamber. As the cryostat is working in magnetic field and the SQUID is also very sensitive to magnetic field, the use of metallic parts will create noisy effect in the results, therefore it is not suitable to use metals in cryostat. The SQUID sensor is mounted and glued on sapphire rod to create a thermal contact with liquid nitrogen as sapphire is good thermal conductor. From the figure: 4.2 it is clear that the sapphire rod along with the SQUID assembly could be adjusted near to 200 µm to sapphire glass window. The sapphire window will prevent heat exchange and allow us to see and adjust the position of SQUID and samples which are very sensitive to low temperature. We can place them near the sensor at distance of 1 mm in case of immunoassays [30]. Focusing the laser on the SQUID in our experimental work the glass window was very advantageous.

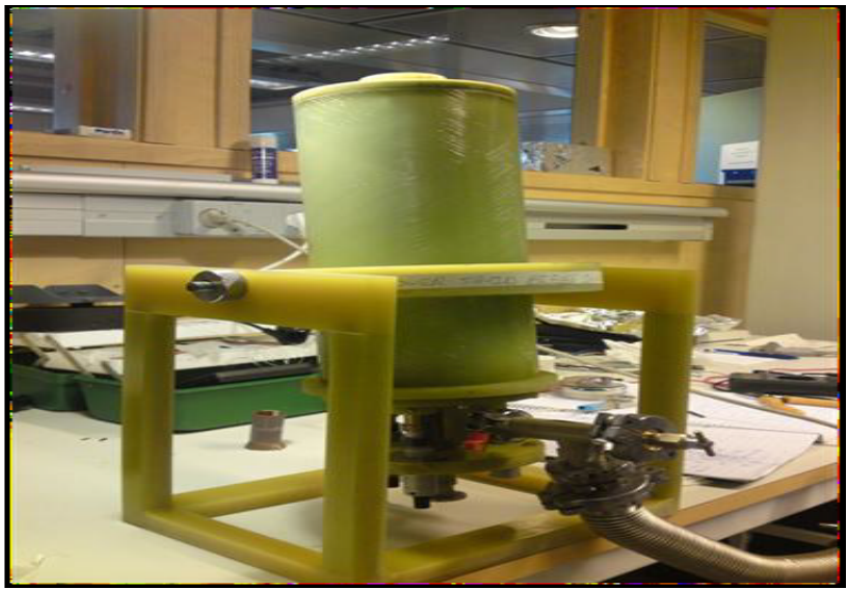

Figure: 4. 1 View of cryostat with vacuum assembly connected [4].

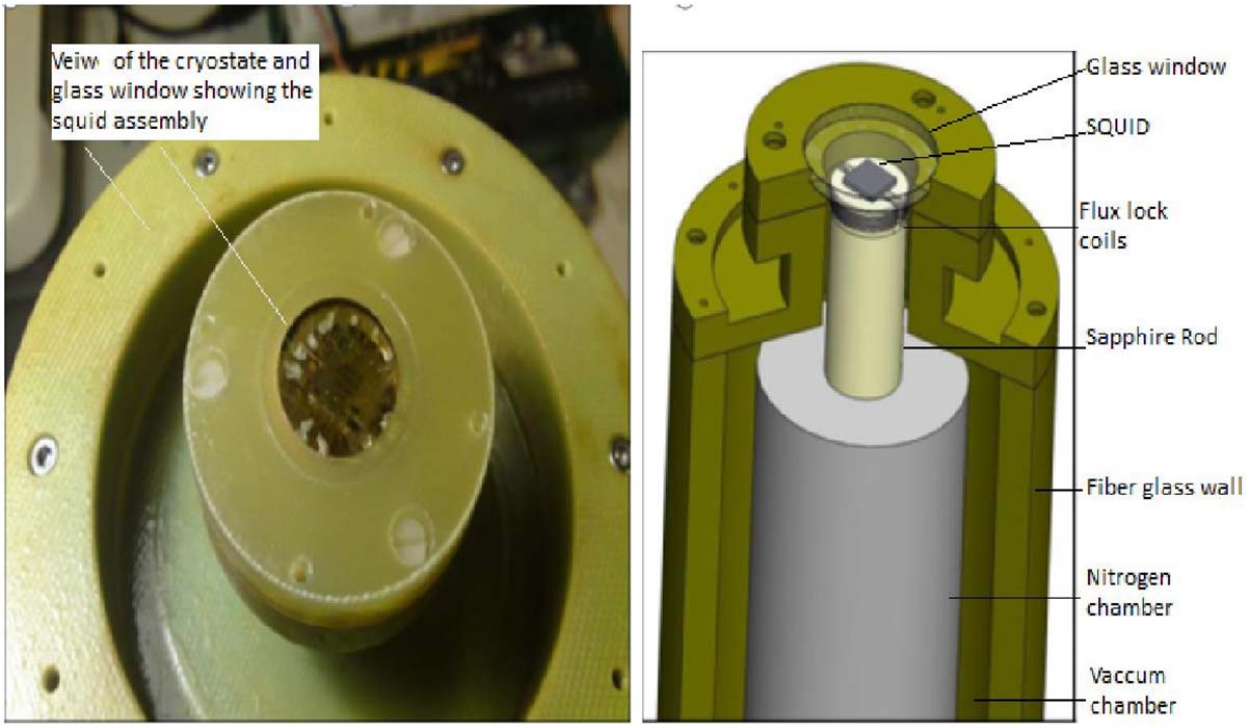

Figure: 4. 2 Upper view of cryostat with glass window and SQUID fitting inside and cross section of cryostat showing whole structure of the system with vacuum chamber flux lock coils SQUID etc. [4].

4.2 Infrared Laser and specifications

We used three lasers; two of them were for testing purpose to check the response of SQUID to infrared lasers heating while from the results of these two lasers we realized we needed to use a third laser with higher power for our required results. The specification of lasers are (1) 850 nm wavelength, maximum power 20 mW, single mode no focusing lens, (2) 1550 nm (max 200 mW) with multi-mode fiber optic without any focusing lens for testing purpose to see the response of SQUID. (3) The Laser we used for the experimental results presented here was 5 W IPG CW Raman laser. We used it with a single mode fiber optic flex core 1060, and the focusing spot size was 10 µm, collimated beam diameter 5 mm, focal length 3 cm, adjustable power (37 dB m), power supply voltage 220 V and output pump current of laser was 1.96 A. The first problem was how to focus the beam on the film, as Infrared wavelength is not visible and the focusing beam spot size was 10 µm. We had to focus the laser manually, after checking the heating response our ultimate goal was to reduce the cooling time. First we had to switch on and off the power supply manually for creating the pulses to see the cooling time. Then we used an optical chopper to create short pulses to get faster heating and cooling and to avoid the extra heating of the YBCO.

4.3 Experimentation and Results

The results presented here is divided in two different sections, the first section is will explain the highlighted results of this study work conducted for fast heating and cooling and the 2nd section is based on the results which were specially conducted to see whether the application of Infrared laser pulses for YBCO film heating in Ulf MRI is compatible with the situation or not, and how much successfully this Infrared laser heating method can be implement in ULF MRI?

4.3.1 Experimentations and Results

By setting up the instrument in RF shielding room and hooking up the data cables with oscilloscope and computer, we were able to adjust the SQUID voltage amplitude and read the data respectively. The bias current of 1 µA was applied to the SQUID and the voltage was monitored continuously, a change in voltage indicated the temperature change of the SQUID. The base temperature was 77 K at this time and then we switched on the high power laser just to see the very first impression of single mode collimated beam. To see the response of SQUID to the power modulation of laser and at the same time it was constantly noticed the oscilloscope to check the temperature change. With increasing power the laser would increase resistance of YBCO film and that was the heating process. The first few experiments took time for the adjustment of focusing laser beam on SQUID as the size of YBCO film was small and infrared laser beam spots was 10 µm. For initial few experiments of the high power laser the applied power range was set as 771 mW because the adjustment of infrared radiation on SQUID

was tricky as it is not visible and the size of SQUID was very small, The SQUID biasing current I_b for the whole experimental procedure was 1 μA, trace time was 20 s. For the next experiments the laser power was changed with each result. During the first few experiments I tried to switch off the laser radiation quick to acquire less cooling time as it was manually switch off and on controlled. The initial problem was the starting of sharp heating of the film from the base temperature to above critical temperature but on the other hand it was noticed from each of the experiment that the faster switching time will get less cooling time. In later experiments we also concentrated on fast heating time of the SQUID.

4.4 Thermometry Function of YBCO

Before the presentation of results it is important to understand the thermometry function of YBCO film. To understand the heating of the YBCO film upto the crictical temprature it is not possible to use any temperature sensor for accurate measurment during the radiation process. For example a diode sensor has a slow response making it inappropriate for such applications. Secondly, if it is placed in between the SQUID and the infrared lasers it will hinder the application of laser radiation on the film. Therefore the temperature was measured as a function of the varying YBCO resistance. For this purpose the calibration of YBCO resistance was executed against a thermister to obtain an R vs T curve which was later used in the experiments as a relative standard. The calibration curve was recorded by enabling the SQUID at room temprature and introducing the liquid nitrogen into the cryostat. The temperature of the YBCO then gradually decreased from room temperature to base temperature(i.e. 82.5 K, also addressed as the superconducting state) shown in figure 4.4 (blue curve).

Lastly, to calculate the temperature a matlab function was generated which gave the temperature as a function of resistance in comparison to the calibration curve. Figure 4. 4 below depicts the matlab function of a test data (red) generated in order to follow the calibration curve (blue). The resultant fuction is given below in the form of equation 4.1 where the transition of resistance R from R < 110 to 0 ohm is infinitely small and remains negligible therefore the reference point from calibration curve to calculate the temperature was considered to be R < 110 ohms. By using this function, the temperature was calculated for all the results obtained during this study.

$$\mathrm{T}(R) = \begin{cases} 82.5 & \mathrm{R} < 110 \\ 2.1\mathrm{e}^{-5}\mathrm{R}^3 - 8.1\mathrm{e}^{-3}\mathrm{R}^2 + 1.1\mathrm{R} + 32 & 110 < \mathrm{R} < 194.8 \\ 0.01\mathrm{R}^2 - 3\mathrm{R} + 299 & 194.8 < \mathrm{R} < 220 \\ 1.7\mathrm{e}^{-3}\mathrm{R}^2 + 2.6\mathrm{R} - 366 & \mathrm{R} > 220 \end{cases} \quad (4.1)$$

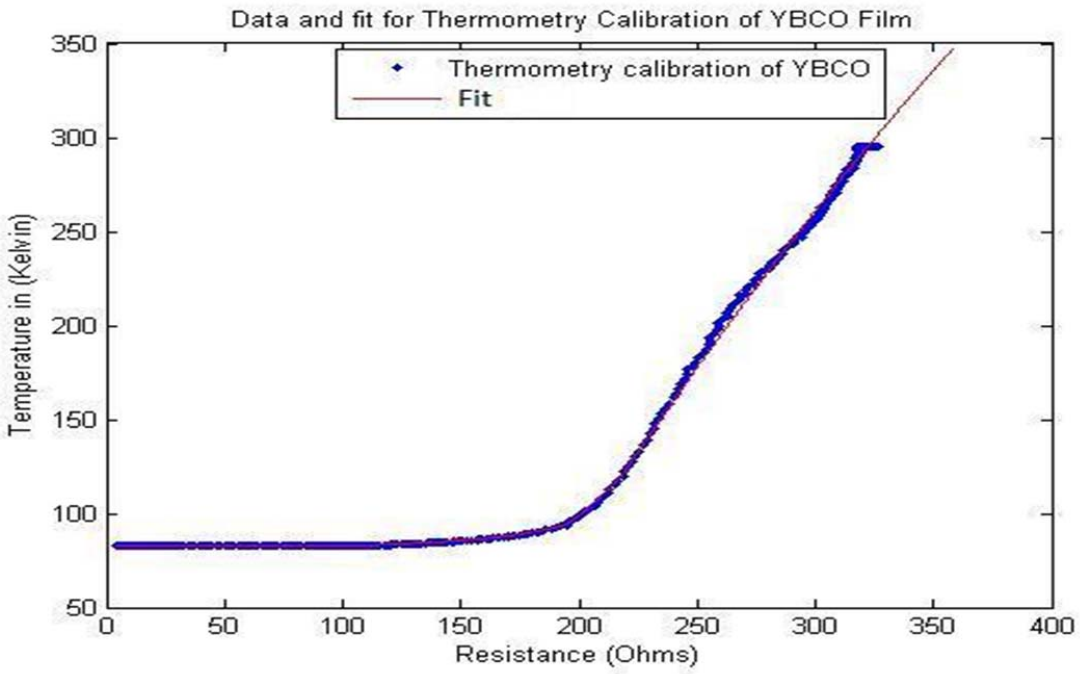

Figure: 4. 3 Showing Temperature vs Resistance, the calibration data (blue) and mat lab function generated for thermometry function and applied sample data results (red).

4.5 Results and discussion

After the initial experiments it was clearly noticed that the short pulses and high power leads to lower cooling times. We therefore added an optical chopper to our setup that would enable rapid toggling of the infrared laser light without having to power it up and down manually. For focusing the pulses on YBCO film, a 3D adjustable stand was used for the best possible results The chopper was placed between focusing lens and the cryostat and a card veiwer was used to find out the exact focal length of the focusing lens. The results achieved during this study work are given below with the best possible cooling time in the experimentation by applying different ranges of laser power. Figure 4.5 showing the results where the minimum power 80 mW with best heating and colling time has been acheived. The results from figure 4.6 have two pulses, the the 2^{nd} pulse heating amplitude is more because the 1st pulse was not completely ended while the 2^{nd} pulse started. Then the cooling time of the 2^{nd} pulse indicates that increasing the laser power will lead to lengthy cooling time~2 ms. We perfomed many experiments and chose a few good results given in the table 4.1 with lowest cooling time and explained it with different reasons. In the table below test No. 4 have two pulses with 280 mW power, the 1st pulse long, it absorbs more energy and does not cool completely. The 2^{nd} pulse is shorter 5.2 ms but the due to high power and lengthy 1^{st} pulse the cooling time of 2^{nd} pulse is long 3.5 ms as compare to the other tests geiven in the table 4.1.

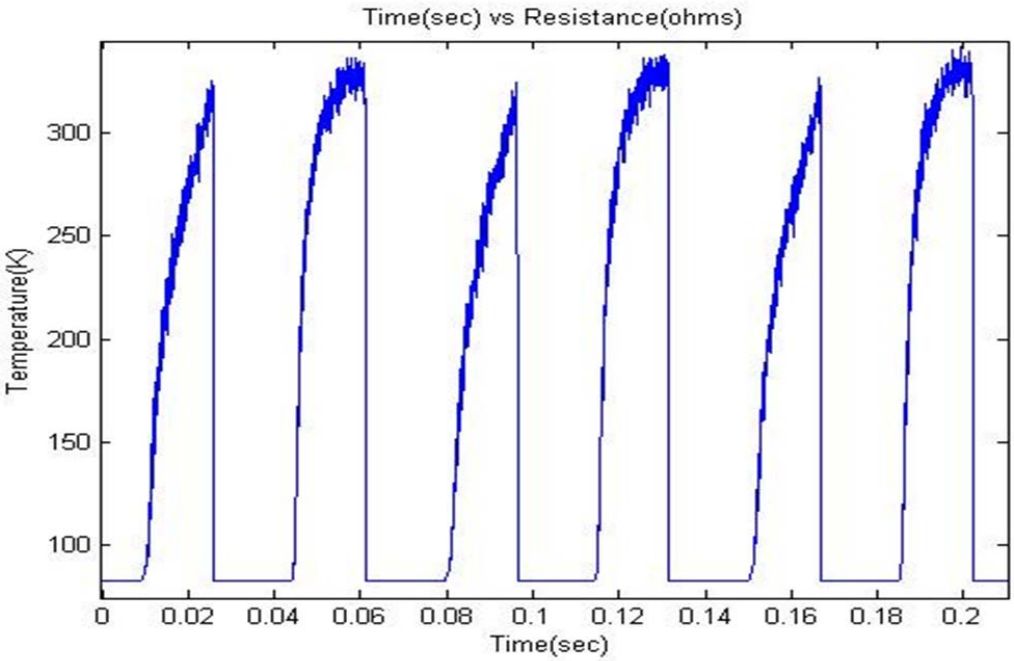

Figure: 4. 4 showing the results with minimum cooling time 1 ms heating time 16.5 ms and minimum applied power 80 mW.

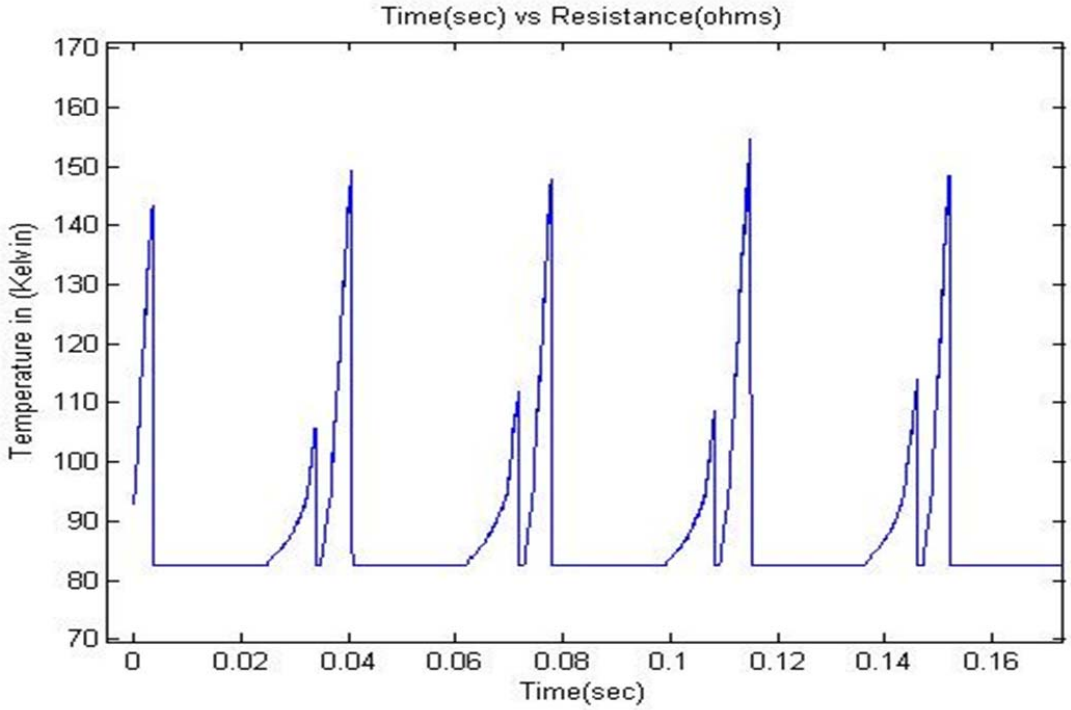

Figure: 4. 5 showing the results with minimum cooling time 2 ms, heating time 16.5 ms and minimum applied power 200 mW.

Table: 4. 1. Summarizing the power applied, cooling time and other specifications for different samples conducted during our experiments, 1 μA SQUID biased current was used during the experiments.

Test No.	Wavelength (nm)	Power (mW)	Cooling time (ms)	Pulse length = heating time (ms)
No. 1	1250 nm	80 mW	1 ms	16.5 ms
No.2	1250 nm	200 mW	1.6 ms	6 ms
No. 3	1250 nm	200 mW	2 ms	16.5 ms
No. 4	1250 nm	280 mW	3.5 ms	5.2 ms

4.6 Experimentation and results for ULF MRI Implementation

The purpose of the experimental results presented in this section was just to check the SQUID response to the laser's first pulse. We wanted to check if the initial pulse can be good enough to heat the SQUID above the critical temperature and how long it will take to heat up by considering its application in ULF MRI. As it showing in figure 4.7 below we got very unsatisfying response from the SQUID initially. Figure 4.7 showing the first test with 260 mW power, it is quite high enough power as compare to the power applied for the results discussed in the earlier section. The first pulse testing results obtained during this was not very promising as it is clear in the figure below because of the focusing of laser in the film. With the increasing the up to 400 mW and focusing more accurately the laser on the film it improved the heating process time. The first pulse heating time was becoming short with every time we increase the laser output power. And the important point was noticed that it did not severely affect the cooling time. But the application of high power started rising the base temperature gradually, and was going up with the timing which is the disadvantage of high power application and leads to lower cooling time in the end.

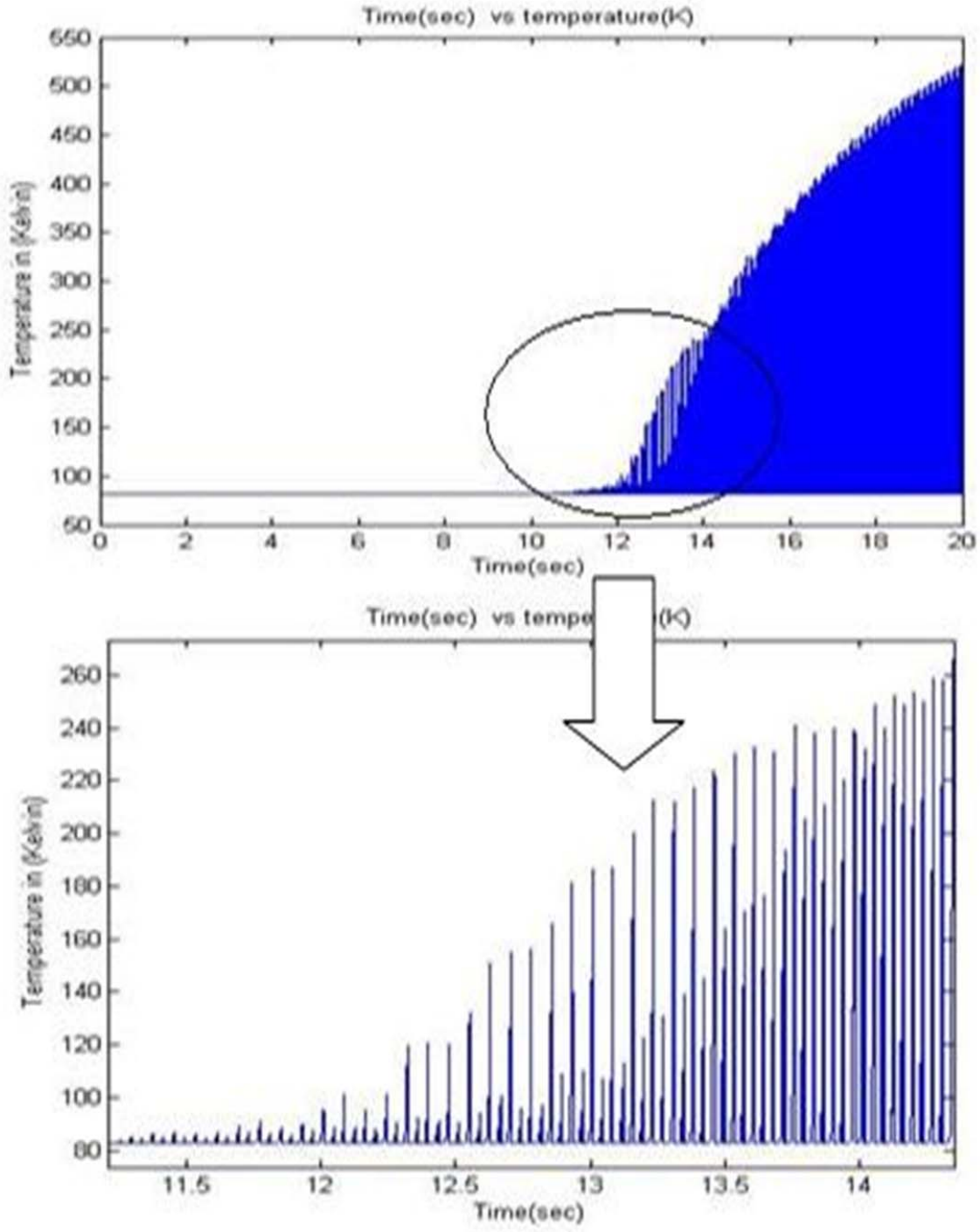

Figure: 4. 6 showing the results for first pulse response of the SQUID to 260 mW power Infrared laser.

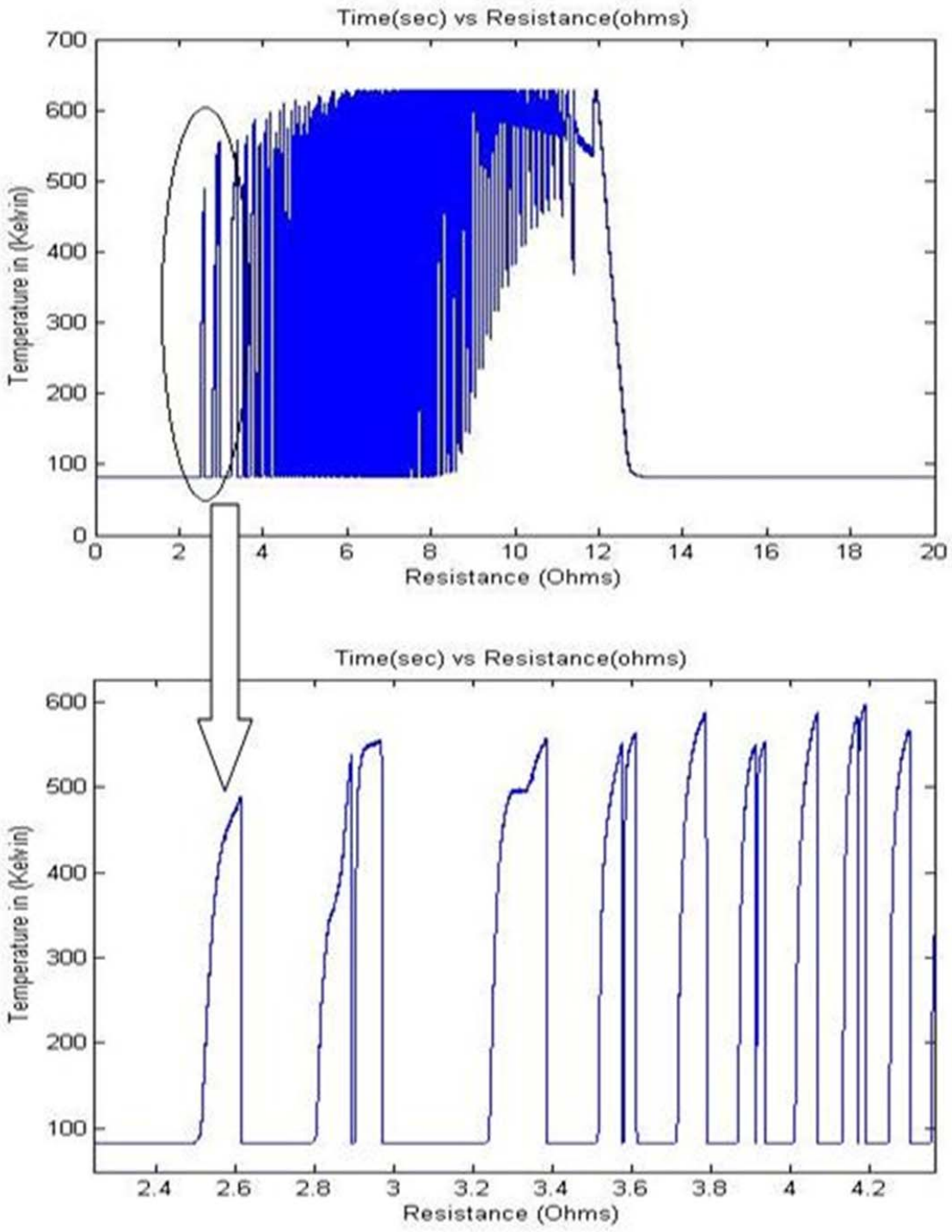

Figure: 4. 7 showing very good response of SQUID to 500 mW power with heating time 211 ms (pulse width) Infrared laser first pulse.

Chapter 5

Discussion and conclusion

With the start of experimental work, the procedure of creating Infrared laser pulses was totally manual. The very first observations were the cooling, and the heating times. Both are directly proportional to the switching of laser pulse and inversely proportional to the applied power. Therefore the first step was to minimize the pulse length; rather we could focus on fast heating. It was investigated that the heating is dependent on laser power and pulse length, our supreme concern was to minimize the cooling time. The other important thing was to overcome the gradual increase of base temperature, the of reason is that even the STO substrate is transparent but continuous absorption of high power laser radiation by YBCO could lead to the exchange of heat between STO and YBCO, results the rise in base temperature and consequently would prolong the cooling time.

Table 5.1 summarizing the results by applying various ranges of laser power to the SQUID and it is clearly showing the relation between the heating time, pulse width and applied power to the SQUID. Although the heating time is still quite long because of testing high power and the manually created long pulse instead of fast smart switching pulses. In the table 5.1 test No. 1, the heating time is not mentioned because of unsatisfied first pulse heating. Test No. 4 showing the dramatic reduction of heating time with the same input power applied as in test No.2, in this result the heating time is six times less than test No.2; this is because of the short pulse duration.

Table 5.1 Summarizing the heating time of different tests

Test	Wavelength (nm)	Power (mW)	Heating time (ms)
No. 1	1250 nm	400 mW	-----
No. 2	1250 nm	400 mW	255 ms
No. 3	1250 nm	500 mW	211 ms
No.4	1250 nm	400 nm	38 ms (short pulse)

While figure 5.1 showing the conclusive demonstration from three different results with stepwise increment in applied power which indicates that the application of high power will increase the cooling time. With the application of low possible input 80 mW power has highest cooling rate 2.18 e5 K/s and shortest 1 ms cooling time among all the results given in chapter 4.. The reason behind low cooling rate (long cooling time) is, when YBCO film absorb high energy it will take longer time to dump it out and cool it back to the base temperature.

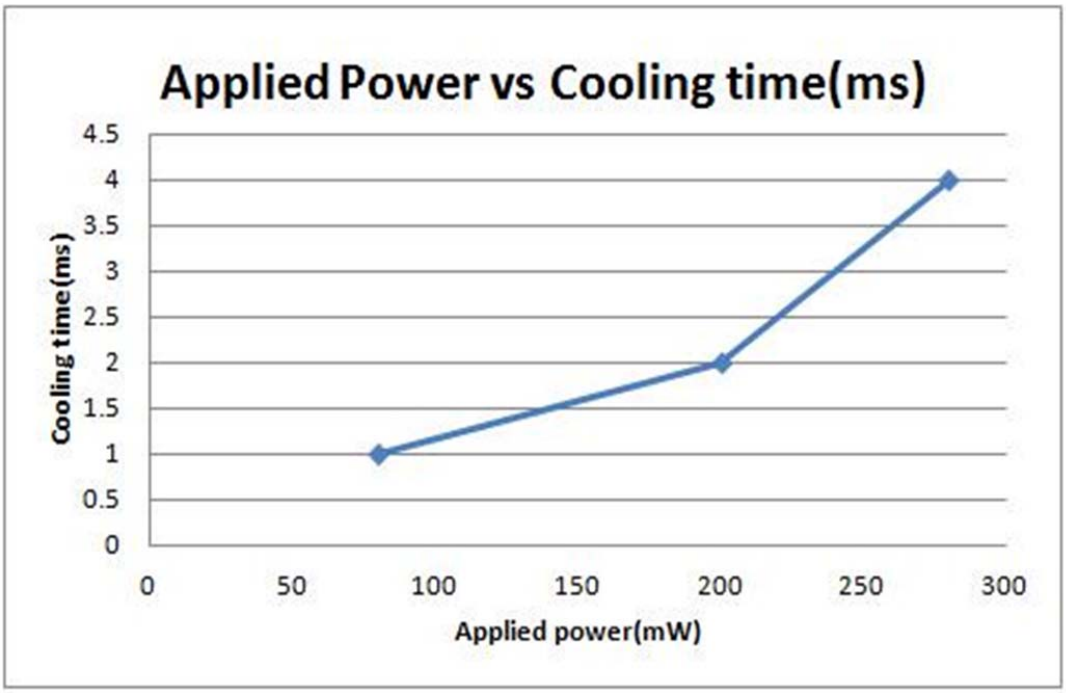

Figure: 5. 1 Indicate that fixed short pulse, high power will have faster heating and cooling with less total energy.

The sole purpose of example from Figure 5.2 is to show that the lowest power application required heat the SQUID up to the critical temperature will reduce the cooling time as it clear in this example with cooling time 10 µs. The lowest cooling time is important for ULF MRI pulse sequence and also the minimum power application of infrared laser can be safe for patient to avoid any possible damages to the skin or eyes during the MRI scanning. Figure 5.2 displays the time (s) vs. resistance (ohms) plot instead of time (s) vs. temperature (K). The function (Equation 4.1) used to fit the calibration curve fails for resistance below 110 ohms because of the rapid change in the resistance over a very narrow temperature range as the film goes through its superconducting transition. However a finite resistance smaller than 110 ohms, can indeed indicate changes in film temperature. We therefore assume the increase in resistance from roughly 5 ohms to over 10 ohms observed in figure 5.2 corresponds to points where the film has warmed above Tc.

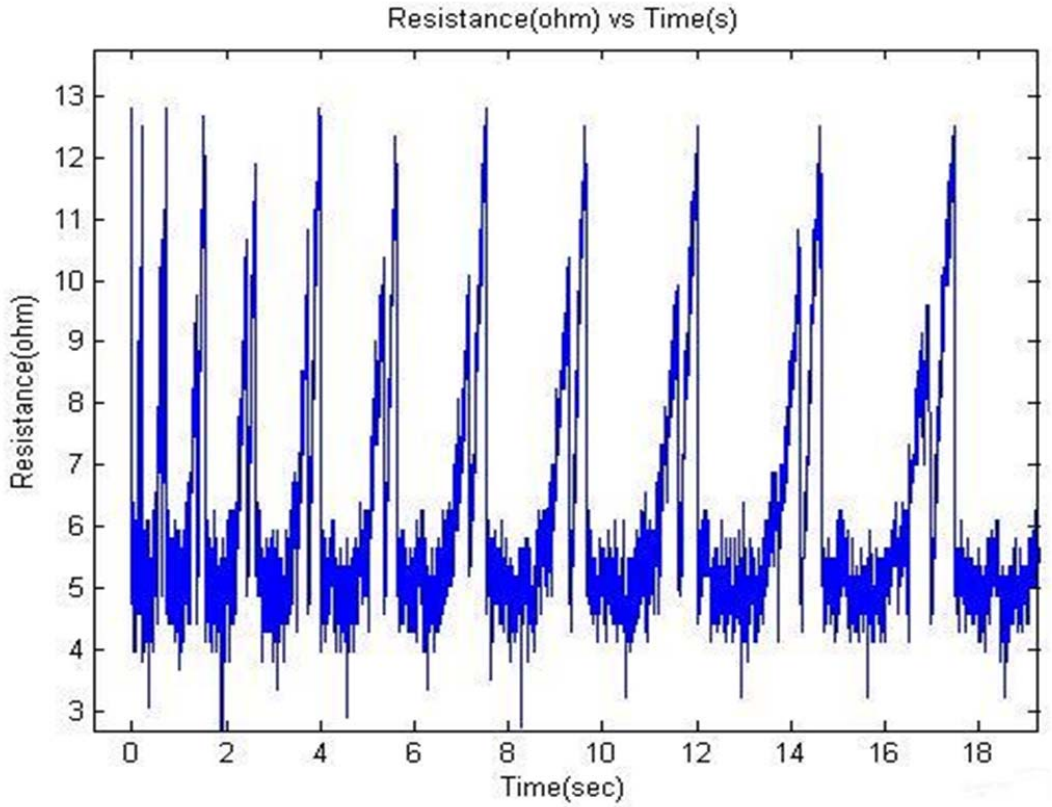

Figure: 5. 2 The Lowest power with shortest pulses will reduce the cooling time more effectively.

The purpose of this project was to see for the proof of principle, whether we could get good enough results by using Infrared laser to get rapid heating and cooling of YBCO, and to ensure the possibility to implement this method in ULF MRI. The ultimate goal was to achieve fast heating but more specifically shortest cooling time of YBCO based SQUID. To achieve the desired results within the range of a few milli to microseconds we found out that adjusting the minimum possible suitable power, shortest pulse width and exact focal length of focusing lens are the obligations. From the results it is clear that the goals are successfully achieved specifically the cooling time within the range of few milli seconds, which was the mile stone of the project and we noticed the possibility of fast heating from results chapter No. 4 section 4. 5 experimentations, specially conducted for the purpose. However there is more possibility to achieve faster heating time as compare to our results and it will be advantage, which totally depends on the pulse width, wavelength (Ideally 1818 nm) of laser and high suitable power. In the case of ULF MRI if the pre-polarization pulse duration is more than 1 s then this achieved heating rates are very good enough.

5.1 Future work

There is a lot of room for the future work in this area and improvement can be done in this regard. Infrared laser's correct wavelength will minimize both heating and cooling time and the real time observation to measure temperature of the film during the radiation procedure will minimize the applied power. Working with fully automatic short pulses, adjustable pre-programmed repetition rate of laser pulses with wavelength near 1818 nm (peak absorption of YBCO) [40] can further improve the results.

The 2nd thing is the incorporation of this method in ULF MRI needs to put more thoughts how to avoid the direct contact of sample or patients with residual Infrared radiation 780 nm - 1400 nm (1250 nm in this study) that can lead to thermal cataract, retinal burn and skin burn injury and if the wavelength is 1.4 µm - 3.0 µm (1818 nm peak absorption of YBCO best option) could cause vitreous humour damage CW > 1 mW laser power and corneal burn CW laser power >1 W [41]. Therefore the above mentioned specification could avoid the maximum laser power application in the system.

Works Cited

[1] Andrei N. Matlashov, Petr L. Volegov, Igor M. Savukov,Michelle A. Espy, John C. Mosher, John J. Gomez, Robert H. Kraus Jr Vadim S. Zotev, "Microtesla MRI of the human brain combined with MEG," *Journal of Magnetic Resonance*, vol. 194, no. 1, 2008.

[2] Clarke John, Hatridge Michael, and Mößle, "SQUID-Detected Magnetic Resonance Imaging in Microtesla Fields," vol. 9, pp. 389–413, August 2007.

[3] Andrei N Matlashov, Petr L Volegov, Algis V Urbaitis, Michelle A Espy and Robert H Kraus Vadim S Zotev, "SQUID-based instrumentation for ultra-low-field MRI," *Superconductor Science and Technology*, vol. 20, no. 11, 2007.

[4] Hadi Arjmandi Tash, "Fast de-trapping of Magnetic Flux from High Temperature Superconducting Devices," Department of Michrotechnology and Nanoscience, Chalmers University of Technology, Gothenburg, Sweden, 2009-2010.

[5] R.E. de Souzaa, K. Schlengab, A. Wong-Foya, R. McDermottb, and A. Pinesa and John Clarke, "NMR and MRI Obtained with High Transition Temperature DC SQUIDs," vol. 10, no. 4, 1999.

[6] R. L. Fagaly, "Superconducting quantum interference device instruments and applications," *Review of Scientific Instruments*, vol. 77, no. 10, October 2006.

[7] L. N. Cooper, J. R. Schrieffer J. Bardeen, "Theory of Superconductivity," *Physical review*, vol. 108, no. 5, December 1 1957.

[8] K. H Bennemann, *Superconductivity: Volume 1: Conventional and Unconventional*, John B. Ketterson, Ed.: Springer, 2008.

[9] Bülent Öktem, "High temperature superconducting YBa2Cu3O7-δ thin films and bolometers," İzmir Institute of Technology, İZMİR, Master thesis May 2006.

[10] J. R. Ashburn, C. J. Torng , P. H. Hor, R. L. Meng, L. Gao, Z. J. Huang, Y. Q. Wang, C. W. Chu M. K. Wu, "Superconductivity at 93 K in a new mixed-phase Y-Ba-Cu-O compound system at ambient pressure," vol. 58, no. 9, 1987.

[11] (2012, january) Superconductivity. [Online]. http://hoffman.physics.harvard.edu/materials/SCintro.php

[12] Robert W. Dull, "Fundamentals of superconductivity," *teachers guide for students*, 1994.

[13] (2012, March) [Online]. http://www.superconductors.org/type2.htm#niobium

[14] Tika Katuwal, "Magnetotransport Studies Of The Mixed State Of Y-Based High Temperature Superconductors," Kent State University, PhD thesis 2007.

[15] HTS Material YBCO. [Online]. http://tfy.tkk.fi/aes/AES/projects/prlaser/material.htm

[16] Georgeta Alecu, "Crystal Structures of Some High-Temperature," vol. 56 , no. 3, pp. 404 - 412, 2004.

[17] (2010, 19 Januray) Yttrium barium copper oxide. [Online]. http://en.wikipedia.org/wiki/Yttrium_barium_copper_oxide

[18] A. E. Koshelev, 1L. N. Bulaevskii, and M. P. Maley, "Josephson coupling, phase correlations, and Josephson plasma resonance in vortex liquid phase," vol. 62, no. 21, December 2000.

[19] (2011, September) SQUID. [Online]. http://hyperphysics.phy-astr.gsu.edu/hbase/solids/squid.html#c3

[20] (2011, September) Wikipedia, Josephson effect. [Online]. http://en.wikipedia.org/wiki/Josephson_effect

[21] Kycia C et al, "A simple three-channel DC SQUID system using time domain multiplexing," *Review of scientific instruments*, vol. 75, no. 8, August 2004.

[22] Dieter Koelle, Frank Ludwig, John Clarke Reinhold Kleiner, "Superconducting Quantum Interference Devices: State of the Art and Applications," vol. 92, no. 10, October 2004.

[23] D. Koelle et al, "High-transition-temperature superconducting quantum interference devices," *Reviews of Modern Physics*, vol. 71, no. 3, pp. 631–686, 1999.

[24] "High-Tc directly coupled direct current SQUID gradiometer with flip-chip flux transformer," *Magnetism and Superconductivity* , vol. 74, no. 9, March 1999.

[25] Hong-Chang Yang, Jau-Han Chen, Shu-Yun Wang, Chin-Hao Chen1, and Jen-Tzong Jeng, "Superconducting Quantum Interference Device: The Most Sensitive Detector of Magnetic Flux," *Tamkang Journal of Science and Engineering*, vol. 9, no. 1, pp. 9-18, 2003.

[26] *Werner Buckel and Reinhold kleiner, Superconductivity fundamentals and applications*, 2nd

ed.: Wiley-VCH Verlag, 2004.

[27] Jean Frederic Isingizwe Nturambirwe, "Superconducting Quantum Interference Device (SQUID) Magnetometers: Principles, Fabrication and Applications," African Institute for Mathematical Sciences (AIMS), Stellenbosch University, South Africa, Postgraduate Diploma 2010.

[28] L. P. Lee, K. Char, M. S. Colclough, and G. Zaharchuk, "Monolithic 77 K DC SQUID magnetometer," *Applied Physics Letters* , vol. 59, no. 23, December 1991.

[29] Neeraj Khare, *Handbook of High-Temperature Superconductor*.: CRC Press, 2003.

[30] Fredrik Öisjöen, "Imnunoassays using high-Tc SQUIDs," Chalmers University of Technology, Gothunburg, Sweden, Thesis for the Degree of Licentiate of Engineering 2009.

[31] Hsiao-Mei Cho, "High-Tc SQUIDs: Noise and Applications," University of Houston, PhD Thesis 2001.

[32] Fredrik Öisjöen, "Development of high Tc SQUID Gradiometers," Chalmers university of technology, Gothenburg, Sweden, Master thesis 2007.

[33] Petr L. Volegov, Andrei N. Matlashov, Igor M. Savukov, Tuba Owens, Vadim S. Zotev, "SQUID-based Microtesla MRI for In Vivo Relaxometry of the Human Brain," *IEEE IEEE Transactions On applied superconductivity*, vol. 19, no. 3, June 2009.

[34] jhon G.webster, *Medical instrumentation application and design*, 3rd ed.

[35] Puig et al, T, "A noval technque to meansure the magnetic relaxation of high temperature superconducting films on ultra short time scales," *Superconductor Science and Technology*, vol. 11, no. 7, pp. 680-685, january 1998.

[36] A. Maniv and E. Polturak, G. Koren, "Observation of Magnetic Flux Generated Spontaneously During a Rapid Quench of Superconducting Films," *Physical Review Letters*, vol. 91, no. 19, April 2003.

[37] P. A. Beasley, R. H. Hammond, M. R. Rosenthal, "Flux noise and flux creep in YBCO thin films," *IEEE Transactions On Magnetics*, vol. 25, no. 2, March 1989.

[38] E. Dantsker, S. Tanaka Clarke, and John, "High-T c super conducting quantum interference devices with slots or holes: Low 1/f noise in ambient magnetic fields," *Applied Physics*

Letters, vol. 70, no. 15, February 1997.

[39] Peter Selders and Roger Wordenweber, "Low-frequency noise reduction in Y-Ba-Cu-0 SQUIDs by artificial defects," *IEEE Transactions on Applied Superconductivity*, vol. II, no. I, March 2001.

[40] EKH Salje H L Dewing, "The effect of the superconducting phase transition on the near-infrared absorption of YBa2Cu3O7-x," *Superconductor Science and Technology*, vol. 5, no. 2, October 1992.

[41] Chalmers Photonic laboratory, "Laser safety," *Course literature in laser engineering*, November 2004.